UCL Université catholique de Louvain

École polytechnique de Louvain (EPL)

epl

Beamforming of large antenna arrays with nulling using L^p-norms for sidelobe minimization

Dissertation presented by
Thibault ETIENNE

for obtaining the master's degree in
Mathematical Engineering

Supervisor(s)
Christophe CRAEYE, François GLINEUR

Readers(s)
Ha BUI VAN, Claude OESTGES

Academic year 2017-2018

Contents

Chapter 1

Introduction

This thesis is closely related to the SKA (Square Kilometer Array) project, which is an international effort aiming to develop the world's largest radio-telescope array. The unprecedented size of this structure will enable providing images from the sky with an extraordinary precision, and help astronomers to improve our understanding of the Universe.

The project is still currently in development phase, and scientific communities from different nationalities collaborate to design the whole system. A few master theses have been conducted on the subject at Université catholique de Louvain in the last years, on various SKA-related topics.

The final SKA structure will consist in an important number of antenna arrays, disseminated around the world in Australia, New Zealand and South Africa, for a total collecting area of 1 square kilometer. A first phase of the project, that will serve to conduct important experiments and calibrations for the final project, is currently in progress and will represent about 10% of the total collecting area. A second phase will then be launched and should be operational in the late 2020's, bringing the radio telescope to its full capacity. More information about this project can be found on its website [1].

In antenna arrays like the SKA, the signals of the different antennas are combined to obtain a global signal proper to the array. This array signal will depend on a lot of parameters (geometry of the array, characteristics of the antennas, ...), and the field studying the way to combining these signals in a clever way to obtain the best array signal characteristics is called beamforming.

In the context of this thesis, we will focus on the relative importance of the antennas in the array signal. Indeed, some excitation currents can be applied to these antennas, acting as weights on the corresponding elements in the global array signal. A lot of methods have already been developed to address this challenge. Among them, this thesis will focus on optimization schemes, which are built to converge iteratively to solutions optimal in a

certain sense.

In our case, the principal objective pursued will be to minimize the signal outside of the main direction, in order to concentrate the most power in this direction of interest. The sidelobe level will be minimized in the general L^p-norm sense, instead of the usual L^∞-norm often encountered in most existing methods.

Besides this, the models developed will also aim to cancel the signal in the directions of important signal sources, like the sun or bright galaxies for instance, in order to avoid them interfering with the signal of interest.

In the next chapter, we are going to recall some important antenna related concepts, necessary to be familiar with the content of this thesis. The third chapter will be dedicated to the beamforming techniques, and an initial optimization model will be developed in this part. The performances of this model will be tested in chapter 4, containing a comprehensive sensitivity analysis of the method and a section dedicated to its robustness. Finally, the last chapter will cover the different additional features that could be implemented to the model, to improve its performances and offer a larger flexibility in the optimization criteria.

Chapter 2

Antenna theory

In this chapter, a brief reminder of some useful concepts will be given in order for the reader to become more familiar with the material of this thesis.

Unlike optical telescopes, that use lenses to form images from the sky in the visible light frequencies (from 430 THz to 770 THz), radio telescopes are antennas working under the radio spectrum (from 3 kHz to 300 GHz). The radio waves present the advantage, among others, of being observable in day time and not being stopped by obstacles such as clouds or interstellar dust particles. Furthermore, they enable astronomers to detect other types of celestial bodies that are usually not seen in the visible frequencies.

To understand the functioning of radio telescopes, let us first look a bit more in depth at the electromagnetic waves behavior. We will then provide a short introduction to antenna theory, and finish with an insight into antenna arrays. All the material of this section is based on the lecture notes of the course LELEC2910 given by C.Craeye at the Université catholique de Louvain [2].

2.1 Electromagnetic waves

2.1.1 Maxwell's equations

Electromagnetic waves refer to the propagation of oscillating magnetic and electric fields through space. In any homogeneous medium, their behavior follows Maxwell's equations, that can be stated as follows :

$$\nabla \times \mathbf{E} = -\frac{\partial \mathbf{B}}{\partial t} \tag{2.1}$$

$$\nabla \times \mathbf{H} = \frac{\partial \mathbf{D}}{\partial t} + \mathbf{J_T} \tag{2.2}$$

$$\nabla \cdot \mathbf{D} = \rho_T \tag{2.3}$$

$$\nabla \cdot \mathbf{B} = 0 \tag{2.4}$$

In these equations, $\mathbf{E}$ and $\mathbf{H}$ denote the electric and magnetic fields respectively, and are related to $\mathbf{D}$ and $\mathbf{B}$ using the following equations :

$$\mathbf{D} = \epsilon \mathbf{E} \tag{2.5}$$

$$\mathbf{B} = \mu \mathbf{H} \tag{2.6}$$

with ϵ the permittivity and μ the permeability of the medium in which the waves are propagating. The terms total $\mathbf{J_T}$ and ρ_T denote the total current and charge densities respectively, and are dependent on the medium characteristics. In a source-free medium, we have $\mathbf{J_T} = 0$ and $\rho_T = 0$, and Maxwell's equations become :

$$\nabla \times \mathbf{E} = -\mu \frac{\partial \mathbf{H}}{\partial t}$$

$$\nabla \times \mathbf{H} = \epsilon \frac{\partial \mathbf{E}}{\partial t}$$

$$\nabla \cdot \mathbf{E} = 0$$

$$\nabla \cdot \mathbf{H} = 0$$

In vacuum (or similarly in the air, as the difference is negligible in this case), we have the following permeability and permittivity constants :

$$\epsilon_0 \approx 8.854 \times 10^{-12} \ [F \cdot m^{-1}]$$

$$\mu_0 \approx 12.566 \times 10^{-7} \ [N \cdot A^{-2}]$$

From this, we can obtain the wave equations for the electric and magnetic fields in the absence of sources :

$$\nabla^2 \mathbf{E} - \mu_0 \epsilon_0 \frac{\partial^2 \mathbf{E}}{\partial t^2} = 0 \tag{2.7}$$

$$\nabla^2 \mathbf{H} - \mu_0 \epsilon_0 \frac{\partial^2 \mathbf{H}}{\partial t^2} = 0 \tag{2.8}$$

2.1.2 Solutions of Maxwell's equations

Depending on the application, Maxwell's equations present different types of solutions. Two examples will be covered in this chapter, the transverse plane waves and the spherical waves.

From now on, we will represent the time varying fields using their phasor notation, which is more practical when we have to deal with waves whose amplitude and frequency are constant with time. Indeed, it makes the dependence to these two parameters implicit, improving the clarity of the computations. If an harmonic field is defined in the time domain by its expression $A\ e^{j(\theta+\omega t)}$, it can be represented in the frequency domain as $A\ e^{j\theta}$, i.e. using its amplitude and its initial phase only. This is what we call its phasor representation.

In order to re-obtain the real field from the phasor expression, one just has to multiply it by the time-varying factor $e^{j\omega t}$ and take the real part of the product :

$$\mathbf{E}(\vec{r},t) = \Re(\vec{E}(\vec{r})e^{j\omega t}) \tag{2.9}$$

Transverse Plane waves

Let us consider waves where both magnetic and electric fields depend only on the direction of propagation (for example the z direction, without loss of generality), in absence of any source. This kind of waves, for which the wavefronts are perpendicular to the propagation direction, is called transverse plane waves. In this situation, the electric field can be written as :

$$\vec{E}(z) = E_x(z)\vec{i_x} + E_y(z)\vec{i_y} + E_z(z)\vec{i_z}$$

It follows from the above equations that $\frac{\partial^2 E_z}{\partial z^2} = 0$, and that the E_z component of the electric field will always be equal to zero. The electric field must therefore be normal to the propagation direction.

In that case, Maxwell's equations admit the following solution :

$$\vec{E}(z) = \vec{E_0}e^{\pm jkz} \tag{2.10}$$

where the condition $k^2 = \omega^2\epsilon_0\mu_0$ must be satisfied, with $k = \frac{2\pi}{\lambda}$ corresponding to the wave number. The expression of the magnetic field H can now be obtained directly from Maxwell's equations, and has a similar form :

$$\vec{H}(z) = \vec{H_0}e^{\pm jkz} \tag{2.11}$$

It can be proven that this magnetic field must similarly be normal to the propagation direction, but also to the electric field.

Spherical waves

Let us now consider the case where electromagnetic waves are emitted from a source point (once again, in a medium without loss). This source will generate spherical waves, whose amplitude decreases with the distance from the source. This kind of waves will be useful later, when we will study the radiation of the antennas.

If we use a polar coordinates referential, we can express the magnetic and electric fields using r, θ and ϕ components. Using the same kind of reasoning as in the previous case, it can be shown that the magnetic and electric fields are normal to each other, and that their propagation direction components (radial in this case) in the far field are equal to zero.

Spherical waves have solutions of the following shape :

$$\vec{E}(r,\theta,\phi) = \frac{\vec{E_0}(\theta,\phi)}{r} e^{\pm jkr} \tag{2.12}$$

$$\vec{H}(r,\theta,\phi) = \frac{\vec{H_0}(\theta,\phi)}{r} e^{\pm jkr} \tag{2.13}$$

where the magnetic field can once again be obtained from the electric field expression along with Maxwell's equations. It is important to note that $\vec{E_0}$ and $\vec{H_0}$ are not necessarily equal in every direction.

Planar waves can be seen as a particular case of the spherical waves, where the distance from the source is so great that we can consider it does not influence the field amplitude anymore.

2.1.3 Wave impedance and Poynting vector

In the previous situations, we made the assumptions that the complex fields amplitudes were constant with time. Therefore, the ratio $\eta = \frac{|E|}{|H|}$, called wave impedance, will also be constant. From the fields expressions obtained above, it can be deduced that

$$\eta = \frac{|E|}{|H|} = \sqrt{\frac{\mu}{\epsilon}} \tag{2.14}$$

In the case of plane waves in free space, the wave impedance is approximately equal to $376.730\,\Omega$.

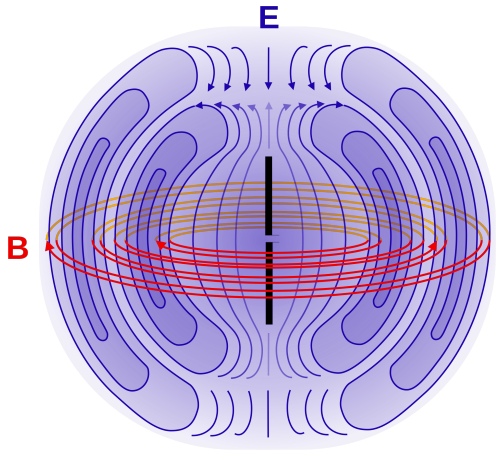

Figure 2.1: Electromagnetic fields generated by a dipole antenna [3]

In order to characterize the signal power in a particular direction, we also introduce the Poynting vector $\mathbf{S} = \mathbf{E} \times \mathbf{H}$, whose amplitude S represents the power density (per surface unit) generated by the fields, which will be useful later when evaluating the radiation pattern of an antenna (i.e. its signal power distribution with the observation direction). For this purpose, it can be interesting to work with a time-averaged value of this amplitude, that can be obtained as :

$$\langle S \rangle = \frac{1}{2\eta} \|\vec{E}\|^2 \tag{2.15}$$

2.2 Antennas behavior

In substance, antennas are conductor components used to transmit or receive electromagnetic waves. They can either convert alternating current into radio waves (transmitters), or alternatively radio waves into current (receivers). The simplest example is the dipole antenna, consisting of two conductor wires, in which alternating current is flowing. This oscillating current generates in turn an oscillating electric field along with a perpendicular magnetic field, accordingly to the fundamental laws of electromagnetism (see figure 2.1).

2.2.1 Reciprocity theorem

A very important theorem of antenna theory (and more generally of the electromagnetism theory) is the Lorentz reciprocity. Formally, this theorem describes the interaction between two current sources and their respective induced fields. If we apply this theorem to the case of antennas, we obtain the interesting result that the characteristics in reception are the same as the ones in transmission. In particular, the radiation pattern of any antenna

will be the same in both cases, which will be useful when studying the behavior of the radio-telescopes.

2.2.2 Antennas characteristics

Every antenna is characterized by several numbers, among the ones detailed below :

- The directivity $D(\widehat{u})$ is the ratio between the Poynting's vector in any direction and the density power that would be radiated if the source was isotropic. If no direction is specified, it is assumed that we consider the direction $\hat{u}$ for which the Poynting's vector is maximal. The antenna directivity can be computed as :

$$D(\widehat{u}) = 4\pi R^2 \frac{S(\widehat{u})}{P_r} \tag{2.16}$$

  with P_r the total radiated power and R the distance from the antenna.

- The gain $G(\widehat{u})$ is defined similarly, taking the total power P_f delivered to the antenna instead of the radiated power :

$$G(\widehat{u}) = 4\pi R^2 \frac{S(\widehat{u})}{P_f} \tag{2.17}$$

  The antenna gain can be obtained simply from the directivity by multiplying it by the antenna's radiation efficiency ν, defined as the ratio between the radiated power and the total power.

2.2.3 Noise

When an antenna functions as a receiver, the intercepted signal is affected by unwanted noise that can interfere with the desired information. This noise can come from external sources (cosmic radiations, signal coming from bright interferers, ...) as well as from internal sources, specific to the antenna. Indeed, as any physical body, antennas and front-end amplifiers emit thermal radiation that will add up to the emitted signal, and potentially blur it.

When designing an antenna, it is important to be able to quantify the noise level of any transmission, and the SNR (ratio between the useful signal power and the noise power) should always be kept as high as possible.

2.2.4 Radiation Pattern

The radiation pattern $\vec{F}(\theta, \phi)$ of an antenna characterizes the directional dependency of its electromagnetic field in the far field :

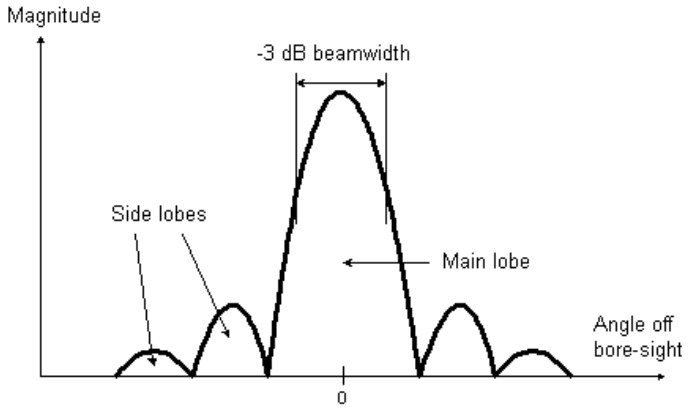

Figure 2.2: Typical example of the radiation pattern of an antenna

$$\vec{E}(r,\theta,\phi) = \vec{F}(\theta,\phi)\frac{e^{jkr}}{r} \tag{2.18}$$

A typical example of radiation pattern can be seen on figure 2.2.

The main lobe is located in the observation direction, where the signal power is maximal. Around this area, we can observe the appearance of sidelobes, whose amplitude decrease with the distance from the main lobe. The level of these sidelobes should be kept minimal, in order not to interfere with the signal of interest. In terms of gain, lowering these sidelobes will ensure a higher gain in the direction of observation. In some cases, there might also be directions where the radiated signal is equal to zero (nulling directions). When designing radio-telescopes, one might want to place these nulls in the direction of very bright interferers (whose positions are known in advance), in order to cancel the corresponding signal.

2.3 Antenna arrays

As seen above, every antenna is characterized by its radiation pattern, which must ideally present a maximal directivity in the desired direction. However, it is possible to combine signals coming from different antennas in order to get a global array signal, with better characteristics that the separate ones.

To achieve this, the antennas (also called elements) are organized into arrays of particular geometries. Antenna arrays can be classified into various types. Among them, we will study the case of the phased arrays, whose maximal directivity direction can be controlled by introducing phase shifts between the different elements according to their relative positions, in order to generate constructive interference and increase the global pattern of

the array in the required direction. When designing the array, one can therefore take advantage of its geometry in order to pursue different objectives (for example lowering the sidelobe level, or increasing the signal to noise ratio). In the context of radio-telescopes, this is what we call astronomical interferometry.

Another important advantage of the arrays over the separate antennas is the fact that they provide a much larger spatial aperture. This will be particularly useful for low frequencies, whose larger wavelengths require similarly larger apertures to transmit and receive the signal properly.

In this section, the antenna array behavior will be described using three principles (superposition, translation and multiplication), that will enable us to build the array pattern under the assumption that every antenna is considered isolated from the others. We will then introduce the mutual coupling effect, which describes the interactions between the elements, in order to obtain patterns that are closer to reality.

2.3.1 Superposition principle

If we denote $\vec{F_i}(\hat{u})$ the radiation pattern of a single antenna i, the global array pattern AP is obtained as :

$$\vec{AP}(\hat{u}) = \sum_{i=1}^{N} \vec{F_i}(\hat{u})$$

This is what we call the superposition principle, resulting from Maxwell's equations linearity (the resulting field is equal to the sum of all the separate fields). Furthermore, if we apply excitation currents on the array antennas, these currents will act as weights on the corresponding elements in the array. If we call w_i the complex excitation current (or weight) on the i^{th} antenna, the array pattern becomes :

$$\vec{AP}(\hat{u}) = \sum_{i=1}^{N} w_i \vec{F_i}(\hat{u}) \tag{2.19}$$

Later, playing with these weights will enable to modify the radiation pattern. Indeed, for a given geometry, optimizing these weights following different objectives and constraints will result in improving the array's characteristics, which will be the central topic of this thesis. The details on the pursued objectives and the modelization will be explained in another section.

2.3.2 Translation principle

In order to understand the effect of the elements positions on the array signal, let us consider two identical antennas placed at two different locations. These antenna will receive the same signal coming from the same direction. However, they will experience a delay due to their relative position, that will result in a phase shift in the received signals. In order to illustrate this, let us call $\vec{F}(\hat{u})$ the radiation pattern of the first antenna, placed at the origin. The second antenna, with a position $\vec{d}$ from the origin, has a radiation pattern $\vec{F'}(\hat{u})$. Suppose now that they are looking toward an object in the very far field, the observation direction $\hat{u}$ can then be considered the same for both antennas. However, the distance from the source will be different : if the first antenna is at a distance r_1 from the source, the distance r_2 between the second antenna and the source can be approximated as :

$$r_2 \approx r_1 - \hat{u} \cdot \vec{d}$$

The second antenna will therefore experience a phase delay compared to the first antenna, corresponding to the distance difference. The radiation vector of the second antenna will be related the one of the first antenna following the relation

$$\vec{F'}(\hat{u}) = \vec{F}(\hat{u})\, e^{jk\hat{u}\cdot\vec{d}} \tag{2.20}$$

2.3.3 Multiplication principle

If we now consider an array of n elements with positions $\vec{r_i}$, the array pattern can be written as :

$$\vec{AP}(\hat{u}) = \sum_{i=1}^{N} w_i \vec{F_i}(\hat{u}) = \sum_{i=1}^{N} w_i \vec{F_0}(\hat{u}) e^{jk\hat{u}\cdot\vec{r_i}}$$

where $\vec{F_0}(\hat{u})$ denotes the radiation pattern of an antenna that would be placed at the origin. In this expression, if we call $R(\hat{u}) = \sum_{i=1}^{N} w_i e^{jk\hat{u}\cdot\vec{r_i}}$ the array factor, the array pattern can be expressed as :

$$\vec{AP}(\hat{u}) = R(\hat{u})\vec{F_0}(\hat{u}) \tag{2.21}$$

where the array factor $R(\hat{u})$ is a scalar function of $\hat{u}$. This multiplication principle could be used again to compute the pattern of an array of arrays, following the same reasoning.

2.3.4 Mutual coupling effect

In the previous sections, we made the assumption that the radiation patterns of all the antennas were the same, up to a phase factor. This amounts to consider that the antennas are completely isolated from each other, and that there is no interference between them. However, if we want to represent the reality more accurately, we cannot ignore the interactions.

We therefore introduce mutual coupling : instead of considering arrays of completely isolated antennas, we will now consider the radiation patterns of each antenna in presence of the other inactive elements (excitation currents equal to zero). Indeed, when an antenna is active in reception, it also radiates in its neighbourhood, exciting other close antennas that emit in turn to their own neighbours.

To model this coupling effect, several methods can be used. Among them, HARP is a technique recently developed at UCL during the last years that will be used in this thesis [4][5]. In order to model the interactions between the antennas, this method uses a Macro-Basis Functions (MBF) approach to represent the currents induced from elements to elements. At first, the interactions between the elements are interpolated using harmonic polynomial functions. The results of these computations can then be used to build what we call the Embedded Element Pattern (EEP) of each element, which is the radiation pattern obtained when taking into account not only the phase shift due to the relative positions of the antennas, but also the mutual coupling effect.

Once the Embedded Element Patterns are known, the Array Pattern can simply be computed as :

$$\vec{AP}(\hat{u}) = \sum_{i=1}^{N} w_i \vec{EEP}_i(\hat{u}) \tag{2.22}$$

When using the Embedded Element Patterns, no use is made of the array factor introduced in the last subsection.

Chapter 3

Optimization models for beamforming

While the previous chapter focused on the phased arrays functioning, this chapter will cover the techniques used to determine which are the optimal weights to apply to each element. A review of the existing beamforming techniques will be made, before detailing the specificities of the models that will be developed in this thesis. At the end of the chapter, a functional optimization model will be exposed, whose performance will be tested in detail in chapter 4, and which will serve as reference before implementing further features in chapter 5.

3.1 Introduction to beamforming

In the context of radio-astronomy, beamforming (or spatial filtering) refers to all the techniques used to combine the signals of the elements of a phased array in a clever way, in order to increase the signal amplitude in some directions (constructive interference), and attenuate it in other directions (destructive interference).

Among the existing techniques, one can distinguish four main categories, as detailed by Barry D. Van Veen and Kevin M. Buckley [6] :

Data independent techniques

This category contains all the techniques in which the weights computation does not depend on the statistics of the array signal. The weights are therefore purely deterministic and are fixed in advance in order to match a desired pattern, and will stay the same for any situation regardless of the signal characteristics. In order for these methods to be efficient, the observation and interferers directions must be known precisely in advance. These

methods are therefore well suited when little is known about the signal characteristics, and they are usually quite robust as they do not depend on the environment conditions.

The simplest form of data independent technique is the conventional beamformer. Its objective is to maximize the gain in the observation direction for a given frequency, without any other constraint. It is of course possible to build far more complex beamformers, by specifying more constraints and different objectives, which will be the target of this thesis.

Statistically optimal techniques

Unlike the previous ones, these techniques require the knowledge of some signal data and statistics in order to optimize particular functions of interest (the SNR or the signal variance, for example) . Usually, for a noisy intercepted signal $\mathbf{x} + \mathbf{n}$, the necessary data involves the signal $\mathbf{x}$ covariance matrix, defined as $R_x = E\left\{\mathbf{x}^H\mathbf{x}\right\}$, and/or the noise $\mathbf{n}$ covariance matrix $R_n = E\left\{\mathbf{n}^H\mathbf{n}\right\}$. While they enable better adaptation to the signal characteristics, they are also highly sensitive to the precision of the available data.

Adaptive techniques

These techniques extend the statistically optimum ones, when the data varies significantly with time. In that case, the weights need to be recomputed frequently to adapt to these changes. While these methods are among the most widely used, they are expensive and require large computational effort, and are therefore not really suitable for very large arrays.

Partially adaptive techniques

This last class follows the same principles as the previous one, except that it uses fewer degrees of freedom in the weights recalibration. This approach enables to reduce the computational time as well as the complexity significantly, at the price of some performance reduction. When designing these techniques, one therefore has to determine the best trade-off between the two.

Further information about these categories and the existing techniques can be found in [7] and [8].

3.2 Thesis specificities

The methods developed in this thesis are part of the data-independent category. Although most of the pre-existing techniques of this category can be qualified of direct, which means

that the weights are obtained trough matrix computations, we will rather use iterative optimization algorithms to converge to some optimal weights.

The spatial filtering optimization methods often follow the same scheme : minimizing the signal amplitude outside the main lobe, while maintaining its amplitude in the main direction to a certain level. A summary of the optimization models developed for beamforming has been made by Lebret & Boyd [9][10].

The methods that will be proposed in this thesis will directly extend the work done by Valentin Hamaide during the 2016-2017 academic year for his own master thesis at the UCL [11]. In this context, he developed an optimization model with the following features :

- **Nulling interference** : Most of the existing spatial filtering techniques enable nulling singular interference sources, as combining multiple signals creates destructive interference in particular directions. However, optimization schemes are well suited for cancelling larger interference areas, by constraining all the discrete directions included in these areas. This is particularly useful when dealing with interferers of large angular size : the sun, for example, has an angular diameter of about half a degree, and in that case nulling only one discrete direction would not be sufficient.
- **Mutual coupling** : Usually, array coupling is considered detrimental to the beamforming techniques, as it can possibly degrade the solutions computed initially. It is therefore mainly studied in order to attenuate its effects. In the case of Valentin Hamaide's model however, the mutual coupling effects are computed in advance and directly integrated in the patterns, in order to make them as close as possible to the reality. The method furthermore takes advantage of the randomness that mutual coupling brings in the element patterns, enabling the creation of more complex array patterns.

The models developed for this thesis will be similar in many points and will maintain these features, but will also present significant differences, the most important being the sidelobe discrimination function : as most optimization schemes (including Valentin Hamaide's) minimize the sidelobe level in the infinity-norm sense, this work will prefer the more general L^p-norm approach, whose peculiarities are described below.

Let us denote $AP(\hat{u})$ the array pattern in a particular direction. We want to minimize the signal amplitude everywhere, except in a region Ω_0 around the observation direction. In the infinity norm sense, the sidelobe level is defined as the highest signal level outside the main region :

$$SLL_\infty = \max_{\Omega \setminus \Omega_0} \Big[|AP(\hat{u})| \Big] \tag{3.1}$$

In the L^p-norm sense however, powers of the signal values are averaged over the whole considered region :

$$SLL^p = \Big[\int_{\Omega \setminus \Omega_0} |AP(\hat{u})|^p \, d\Omega \Big]^{\frac{1}{p}} \tag{3.2}$$

The infinity norm approach can hence be seen as a limit case of the L^p-norm where $p \to \infty$.

The L^p-norm choice presents the advantage of lowering the signal amplitude more globally : when minimizing the infinity norm, only the highest signal level will be lowered, resulting in a pattern where a large subset of the discrete directions will be close to that value; with the L^p-norm however, an averaged sum of powers will be considered, enabling a locally higher signal in specific regions for a globally lower signal elsewhere. Furthermore, we will see that the L^p-norm formulation objective is differentiable, which can be highly appreciated when searching for optimal solutions. However, this feature will not be used in the context of this thesis as we will see that the problem convexity will offer even better guarantees and will enable solving the problem more efficiently.

The L^p-norm approach has already been mentioned in the literature [12], including the work of Thibault Clavier et al. for the SKA project in 2014 [13], but has not been studied a lot due to the complexity brought by its formulation. Among the references found on the subject, none of them considered the mutual coupling effect in their computations.

In the next section, an initial model compiling all these features will be proposed.

3.3 Model formulation

3.3.1 Problem definition

Array geometry

Throughout this thesis, we will aim to solve the following generic problem. We consider an array of n antennas, placed at known and fixed positions (x_i, y_i). More specifically, we will study the case of a SKA low-frequency aperture array (LFAA) [14], designed to cover the low-frequency range of the radio-telescope (from about 50 MHz to 350 MHz), but the same method could be applied for any type of array.

The signal behavior strongly depends on the array geometry, and many configurations have been proposed to optimize some array characteristics [13][15]. However, determining these configurations is out of the scope of this thesis. Typically, the LFAA will follow a non-regular distribution [14], in which the positions are randomized with specific algorithms, under particular distance rules. Indeed, the antennas should not be too distant from each

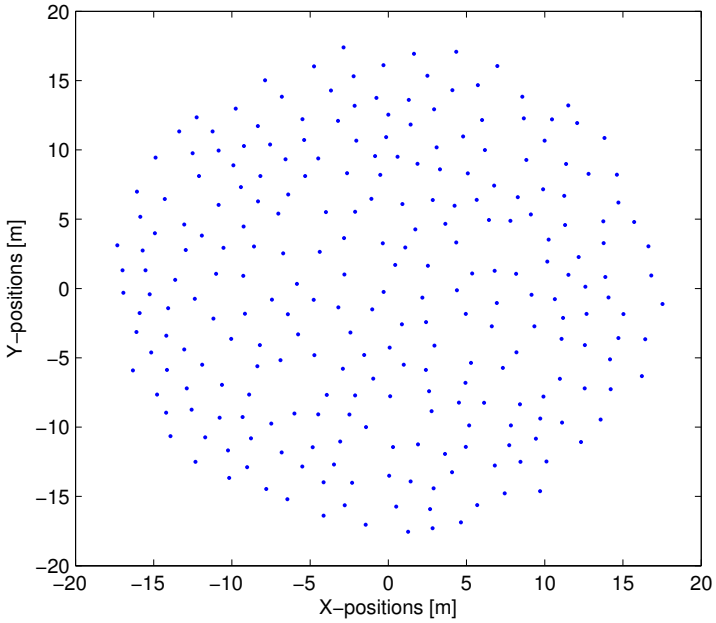

Figure 3.1: Example of non-regular array geometry

other in order to respect the Nyquist criterion, but they cannot be too close either for obvious physical reasons.

This kind of geometry enables better randomization of the mutual coupling effect. An example of such a distribution is shown in figure 3.1.

Element patterns

In the considered array, the element patterns in the presence of mutual coupling are computed in advance, using the HARP software mentioned above [4], for a set of discrete directions (θ, ϕ). The polar angle of observation θ varies from 0° to 90°, and the azimuthal angle of observation ϕ varies from 0° to 360°, forming a semi-spherical observation region Ω, with discretization steps defined by the user according to the required precision (this part will be covered in a specific section in the next chapter).

Array calibration

As explained above, the array pattern expressing the directional dependency of the array signal can be obtained as a sum of the element patterns, weighted by the excitation currents

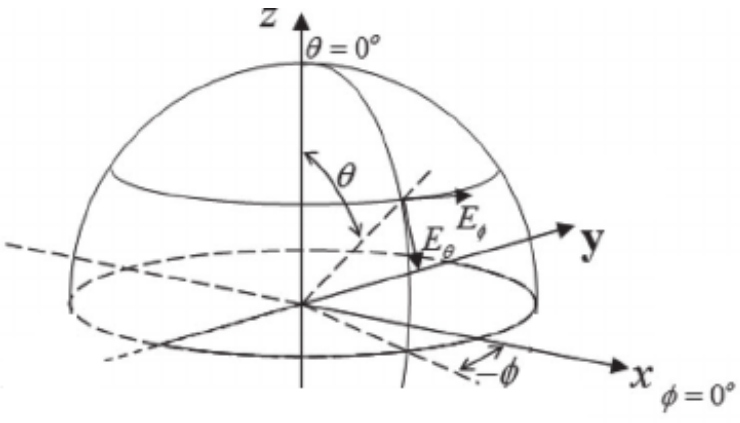

Figure 3.2: Spherical system of coordinates

applied to the corresponding antennas (equation 2.19). The beamforming weights will be the variables of our problem.

The requirements on the pattern are the following : first of all, the signal has to be maximal in the direction of observation (θ_0, ϕ_0). The main lobe will be formed in a region Ω_0 around this direction, whose size can be decided in accordance with specific rules involving the array size and the frequency. Furthermore, in order to improve the array directivity, the pattern level should minimized everywhere outside this region Ω_0, which will be formulated by our objective function.

Finally, we consider possibly multiple sources of interference, coming from directions (θ_i, ϕ_i). We define regions Ω_i around these directions, whose size depend on the sources size, where the signal should be constrained under a small arbitrary level. It is not necessary in our case to impose exact cancellation of the pattern, as sufficiently small values will prevent interference with the signal of interest (the calibration of this value will be discussed later).

3.3.2 Introduction to Convex and and Second Order Cone Programming

The kind of optimization problems described above require the use of many constraints and variables (one complex value for each weight, in addition to the auxiliary variables), which can quickly result in a huge computational time. We must therefore ensure that, for our particular model, there exist algorithms able to find optimal solutions, and this within reasonable time.

For this reason, our model will be formulated as a convex problem. Let us first recall a few definitions about convex programming before going further (this section is based on the course LINMA2471 given by F.Glineur at the Université catholique de Louvain [16]).

Definition 3.1 *A **set** S is called **convex** if it contains every segment connecting two of*

its points

Definition 3.2 *A **function** f is **convex** if its domain is convex, and if* $\forall x, y \in$ dom f, $\forall \alpha \in [0,1]$ *we have the following property :*

$$f(\alpha x + (1-\alpha)y) \leq \alpha f(x) + (1-\alpha) f((y)$$

Convex optimization refers to all the problems minimizing convex functions over convex sets of constraints. Convex problems present the advantage of being solvable in polynomial time[1], and the optimum attained is guaranteed to be global. Furthermore, the particular duality properties of convex programs can be exploited by efficient algorithms to converge faster to optimal solutions.

Inside this class of problems, one particular type of formulation will be useful for the problem modelization : Second Order Cone Programming (SOCP). Once again, let us remind some useful concepts :

Definition 3.3 *The subset* $K \in \mathbb{R}^n$ *is a **cone** if it is closed under scalar multiplication :*

$$\forall x \in K, \forall \alpha \geq 0 : \alpha x \in K$$

Furthermore, the cone K is convex if it is also closed under addition :

$$\forall x, y \in K, \forall \alpha, \beta > 0 : \alpha x + \beta y \in K$$

A particular case of convex cone is the Lorentz cone, or second order cone :

Definition 3.4 *The **Lorentz cone** is the particular type of cone satisfying :*

$$\mathbb{L}^n = \left\{ (x_0, ..., x_n) \in \mathbb{R}^{n+1} \mid \sqrt{x_1^2 + ... + x_n^2} \leq x_0 \right\}$$

It is interesting to note that the Lorentz cone admits a convenient alternative definition, called the rotated cone. By using an appropriate change of variables, we obtain the following set :

Definition 3.5 *The **rotated second order cone** is the particular type of cone satisfying :*

$$\mathbb{L}_r^n = \left\{ (x_0, ..., x_n) \in \mathbb{R}^{n+1} \mid x_2^2 + ... + x_n^2 \leq 2x_0 x_1, \;\; x_0, x_1 \geq 0 \right\}$$

Optimization of a linear objective over a set of linear and second order cone constraints is called Second Order Cone Programming (SOCP), and very efficient solvers exist for this particular class of convex problems. In particular, interior-point solvers converge to a guaranteed solution in a few dozens iterations, and can be successfully applied to problems involving thousands of variables.

[1] In a very large majority of problems encountered in practice

More information about convex optimization in general can be found in [17]. The next section will be dedicated to the way our formulation will be built, ensuring that it stays in the Second Order Cone Programming framework.

3.3.3 Constraints/Objective formulation

Array pattern expression

Before formulating a second order cone program that will contain all the necessary constraints over the array pattern, it is first necessary to express this array pattern in terms of the weights and the available data on the element patterns.

Let us denote by $\mathbf{P}(\theta, \phi)$ the vector of element patterns for a particular direction. The corresponding array pattern can be obtained as the product $AP(\theta, \phi) = \mathbf{P}(\theta, \phi) \cdot \mathbf{w}$. As this expression is a product of complex terms, it can be decomposed into its real and complex parts the following way :

$$\begin{aligned}\mathbf{P} \cdot \mathbf{w} &= (\mathbf{P}^r + i\mathbf{P}^{im}) \cdot (\mathbf{w}^r + i\mathbf{w}^{im}) \\ &= \mathbf{P}^r \cdot \mathbf{w}^r - \mathbf{P}^{im} \cdot \mathbf{w}^{im} + i(\mathbf{P}^r \cdot \mathbf{w}^{im} + \mathbf{P}^{im} \cdot \mathbf{w}^r)\end{aligned}$$

Its amplitude is therefore equal to :

$$|\mathbf{P} \cdot \mathbf{w}| = \sqrt{(\mathbf{P}^r \cdot \mathbf{w}^r - \mathbf{P}^{im} \cdot \mathbf{w}^{im})^2 + (\mathbf{P}^r \cdot \mathbf{w}^{im} + \mathbf{P}^{im} \cdot \mathbf{w}^r)^2} \tag{3.3}$$

In the case of the LFAA, the element patterns are computed along two polarizations [14]. The first one, called horizontal polarization, corresponds to the ϕ-component of the signal. The other one, called vertical polarization, is therefore the θ-component of the signal. If we denote by $\mathbf{P}_H$ and $\mathbf{P}_V$ the horizontal and vertical polarizations computed for every antenna, the global array signal amplitude can be obtained as :

$$\begin{aligned}|AP| &= \sqrt{|AP_H|^2 + |AP_V|^2} \\ &= \sqrt{|\mathbf{P}_H \cdot \mathbf{w}|^2 + |\mathbf{P}_V \cdot \mathbf{w}|^2}\end{aligned}$$

If we substitute the equation 3.4. into this expression, we finally obtain :

$$|AP| = \sqrt{{Z_H^r}^2 + {Z_H^{im}}^2 + {Z_V^r}^2 + {Z_V^{im}}^2} \tag{3.4}$$

where we set the following auxiliary variables for better readability (as these auxiliary variables depend linearly on w, they do not impact the convexity of the formulation) :

$$
\begin{aligned}
Z_H^r &= \mathbf{P}_H^r \cdot \mathbf{w}^r - \mathbf{P}_H^{im} \cdot \mathbf{w}^{im} \\
Z_H^{im} &= \mathbf{P}_H^r \cdot \mathbf{w}^{im} + \mathbf{P}_H^{im} \cdot \mathbf{w}^r \\
Z_V^r &= \mathbf{P}_V^r \cdot \mathbf{w}^r - \mathbf{P}_V^{im} \cdot \mathbf{w}^{im} \\
Z_V^{im} &= \mathbf{P}_V^r \cdot \mathbf{w}^{im} + \mathbf{P}_V^{im} \cdot \mathbf{w}^r
\end{aligned}
$$

Now that we have an expression for the array pattern amplitude, it becomes possible to model the objective pursued as well as the problem constraints.

Sidelobe minimization

As explained above, the objective of the problem is to minimize the sidelobe level in the L^p-norm sense, which can be formulated into a second order cone program [18][19]. As taking the p^{th} root of a positive quantity is a monotonic transformation, minimizing the expression described in equation 3.2 is equivalent to minimize the following function :

$$\int_{\Omega \setminus \Omega_0} |AP(\theta, \phi)|^p d\Omega$$

Integrating explicitly over θ and ϕ, we obtain :

$$\iint_{\Omega \setminus \Omega_0} |AP(\theta, \phi)|^p \sin(\theta) d\theta d\phi$$

Finally, as we integrate over a discrete domain, the minimization function can be approximated by :

$$\sum_{\Omega \setminus \Omega_0} |AP(\theta, \phi)|^p \sin(\theta) \tag{3.5}$$

For any rational p, it is possible to convert this formulation into an equivalent second-order cone program [18]. For example, let us consider the case $p = 4$. Using the signal amplitude expression of equation 3.4, the minimization function can be expressed as :

$$\sum_{i \in \Omega \setminus \Omega_0} |AP(\theta, \phi)|^4 \sin(\theta) = \sum_{i \in \Omega \setminus \Omega_0} ({Z_{H,i}^r}^2 + {Z_{H,i}^{im}}^2 + {Z_{V,i}^r}^2 + Z_{V,i}^{im2})^2 \sin(\theta) \tag{3.6}$$

The problem can therefore be formulated, using the auxiliary variables s_i, as :

$$
\begin{aligned}
&\text{minimize} && t \\
&\text{subject to} && \sum_{i \in \Omega \setminus \Omega_0} s_i \sin(\theta) \leq t \\
& && ({Z^r_{H,i}}^2 + {Z^{im}_{H,i}}^2 + {Z^r_{V,i}}^2 + {Z^{im}_{V,i}}^2)^2 \leq s_i \qquad \text{on } \Omega
\end{aligned}
$$

In this model, the last constraint can be modeled using two successive sets of second order cones :

$$
\begin{cases}
x_i^2 \leq s_i & \text{on } \Omega \\
{Z^r_{H,i}}^2 + {Z^{im}_{H,i}}^2 + {Z^r_{V,i}}^2 + {Z^{im}_{V,i}}^2 \leq x_i & \text{on } \Omega
\end{cases}
$$

Eventually, we obtain the following Second Order Cone Program :

$$
\boxed{
\begin{aligned}
&\text{minimize} && t && \\
&\text{subject to} && \sum_{i \in \Omega \setminus \Omega_0} s_i \sin(\theta) \leq t && \\
& && x_i^2 \leq s_i && \text{on } \Omega \\
& && {Z^r_{H,i}}^2 + {Z^{im}_{H,i}}^2 + {Z^r_{V,i}}^2 + {Z^{im}_{V,i}}^2 \leq x_i && \text{on } \Omega
\end{aligned}
}
$$

In this model, the second and third constraints satisfy the rotated Lorentz cones definition 3.5, where we forced the value of the variable x_0 to 0.5. As the objective function is linear, and all the constraints are either linear or second order cones, the formulation can indeed be cast into SOCP. This approach is well suited and straightforward when p is a power of 2, as it only requires to add a set of new variables and the corresponding cones to extend this formulation to the next power. However, for other values of p, the construction becomes trickier, as the formulation is usually not unique an can potentially require the definition of a lot of cones and variables. An additional example for $p = 6$ is provided in Appendix A.

Main lobe constraints

In addition to the sidelobe minimization, it is necessary to impose the signal amplitude to be maintained to a certain level in the observation direction, otherwise the trivial optimal solution would be to set all the weights to zero. Any arbitrary value could be chosen for this level, as this would only change the order of magnitude of the pattern (taking a twice bigger value would result in a twice bigger pattern amplitude everywhere, and

therefore twice bigger weights). Without loss of generality, we will constrain it to unity. The corresponding constraint would therefore have the following shape :

$$\sqrt{Z_H^r(\theta_0,\phi_0)^2 + Z_H^{im}(\theta_0,\phi_0)^2 + Z_V^r(\theta_0,\phi_0)^2 + Z_V^{im}(\theta_0,\phi_0)^2} = 1$$

However, while imposing upper bounds on euclidian norms can be modeled using second order cones, imposing lower bounds or equality constraints on these norms is unfortunately not possible using convex constraints. To get around this problem, a possible solution is to enforce the value of the co-polarization of the signal instead.

The co-polarization, or reference polarization, of an antenna is the polarization in which the antenna is meant to radiate the most power (or similarly receive, because of the reciprocity principle). Similarly, the cross-polarization is the signal component orthogonal to the co-polarization. In the case of the SKA low-frequency arrays, the antennas are designed to have a very low cross-polarization [14], and the co-polarization amplitude will therefore stay very close to the whole signal amplitude.

Different approaches have been proposed to compute the co and cross-polarization in terms of the vertical and horizontal ones [20]. Among them, the widespread "Ludwig-3" definitions of the co and cross-polarizations are stated as follows :

$$\begin{cases} \hat{e}_{co} = \cos(\phi)\,\hat{e}_V - \sin(\phi)\,\hat{e}_H \\ \hat{e}_{cross} = \sin(\phi)\,\hat{e}_V + \cos(\phi)\,\hat{e}_H \end{cases} \tag{3.7}$$

where the angle ϕ is computed from the antenna reference direction in the X-Y plane. In fact, it is possible to be more general and to let the user decide on its own version of the co-polarization. Using two coefficients α and β (possibly complex) satisfying the property $|\alpha|^2 + |\beta|^2 = 1$, the new co/cross-polarizations definitions become :

$$\begin{cases} \hat{e}_{co} = \alpha\,\hat{e}_V + \beta\,\hat{e}_H \\ \hat{e}_{cross} = -\beta\,\hat{e}_V + \alpha\,\hat{e}_H \end{cases} \tag{3.8}$$

Any desired polarization can be achieved by varying the α, β coefficients. While keeping the coefficients real will yield only linear polarizations, using complex values will enable generating elliptical polarizations as well.

Regardless of the chosen definition, the array pattern co-polarization is consequently equal to :

$$\mathbf{P}_{co} \cdot \mathbf{w} = \alpha\,\mathbf{P}_V \cdot \mathbf{w} + \beta\,\mathbf{P}_H \cdot \mathbf{w}$$

As this expression is a complex product, the same reasoning as above can be applied to separate the real and imaginary parts. Finally, imposing the co-polarization signal to the complex number 1 amounts to equal its real part to 1 and its imaginary part to 0 :

$$\mathbf{P}_{co}^{r} \cdot \mathbf{w}^{r} - \mathbf{P}_{co}^{im} \cdot \mathbf{w}^{im} = 1 \tag{3.9}$$

$$\mathbf{P}_{co}^{r} \cdot \mathbf{w}^{im} + \mathbf{P}_{co}^{im} \cdot \mathbf{w}^{r} = 0 \tag{3.10}$$

At this point, one could ask whether generality is lost by fixing the co-polarization signal value exactly to 1 rather than constraining only its amplitude (and therefore allowing it to take any value on the complex unitary circle). As all the element patterns oscillate with the same frequency, the whole array pattern will be defined up to a phase factor, and setting a particular phase for the pattern in a particular direction (the main direction in our case), will only result in setting a particular phase for the whole pattern. Therefore, taking another arbitrary value on the complex circle would yield the same weights, only shifted by the corresponding phase factor.

Signal cancellation constraints

As explained above, setting upper bounds on euclidian norms can be achieved simply using second order cones, by setting the right-term variables of definition 3.5 to the adequate values. In order to cancel the signal coming from large interference sources, the array pattern can therefore be constrained to an arbitrary small constant in the discrete directions contained in the angular regions Ω_i around these sources :

$$\sqrt{{Z_H^r}^2 + Z_H^{im2} + {Z_V^r}^2 + Z_V^{im2}} \leq C \qquad \text{on } \Omega_i$$

This problem can even be tackled more simply by using the auxiliary variable x_i defined in the sidelobe minimization section. As these variables are constrained to be greater than the square of the signal amplitude, the previous constraint can be re-written as :

$$x_i \leq C^2 \qquad \text{on } \Omega_i \tag{3.11}$$

This way, the signal cancellation is achieved through linear constraints instead of cones, lightening the formulation and reducing the necessary amount of computations.

Main lobe window

Finally, a last set of constraints is necessary to control the shape of the main lobe, and avoid encountering too important sidelobes near the main region. To do so, we will once

again impose upper bounds on the array pattern. In the region Ω_0 (a ball of angular radius r around the main direction), the signal power will be kept under the unity, to ensure that the signal level will indeed stay maximal in the main direction.

Just outside this region (but still in a ball Ω_{hp} of angular radius $1.5\,r$ around the main direction), the signal level will kept under 0.5. This way, we will be able to control the size of the main lobe, by imposing the radius at which the signal power is equal to half the maximal power.

$$x_i \leq 1 \qquad \text{on } \Omega_0 \tag{3.12}$$

$$x_i \leq 0.5 \qquad \text{on } \Omega_{hp}\backslash\Omega_0 \tag{3.13}$$

Complete Model (for $p = 4$)

To summarize all the above considerations, the whole model with the entire set of constraints can be found below :

$$\begin{aligned}
&\text{minimize} && t && \\
&\text{subject to} && \sum_{i\in\Omega\backslash\Omega_0} s_i \sin(\theta) \leq t && \\
& && x_i^2 \leq s_i && \text{on } \Omega \\
& && {Z^r_{H,i}}^2 + {Z^{im}_{H,i}}^2 + {Z^r_{V,i}}^2 + {Z^{im}_{V,i}}^2 \leq x_i && \text{on } \Omega \\
& && Z^r_H = \mathbf{P}^r_H \mathbf{w}^r - \mathbf{P}^{im}_H \mathbf{w}^{im} && \text{on } \Omega \\
& && Z^{im}_H = \mathbf{P}^r_H \mathbf{w}^{im} + \mathbf{P}^{im}_H \mathbf{w}^r && \text{on } \Omega \\
& && Z^r_V = \mathbf{P}^r_V \mathbf{w}^r - \mathbf{P}^{im}_V \mathbf{w}^{im} && \text{on } \Omega \\
& && Z^{im}_V = \mathbf{P}^r_V \mathbf{w}^{im} + \mathbf{P}^{im}_V \mathbf{w}^r && \text{on } \Omega \\
& && \mathbf{P}^r_{co} \cdot \mathbf{w}^r - \mathbf{P}^{im}_{co} \cdot \mathbf{w}^{im} = 1 && \text{for } (\theta_0, \phi_0) \\
& && \mathbf{P}^r_{co} \cdot \mathbf{w}^{im} + \mathbf{P}^{im}_{co} \cdot \mathbf{w}^r = 0 && \text{for } (\theta_0, \phi_0) \\
& && x_i \leq C^2 && \text{on } \Omega_i \\
& && x_i \leq 1 && \text{on } \Omega_0 \\
& && x_i \leq 0.5 && \text{on } \Omega_{hp}\backslash\Omega_0
\end{aligned}$$

Chapter 4

Results and sensitivity analysis

This chapter will be dedicated to the performance analysis of the model presented previously. In order to test the dependency of the solutions obtained with the algorithm to the parameters, we will perform a comprehensive sensitivity analysis in the first section. We will later estimate the robustness of the method, and how it could be improved, and finally study the benefits of taking the mutual coupling effects into account into our computations

4.1 How to test the solution ?

4.1.1 Indicators of the solution properties

When running the algorithm on a particular instance, different indicators can help us to characterize the solution obtained. Four of them will be studied more particularly : the sidelobe level, the SNR, the array directivity and the algorithm execution time.

Sidelobe level

Among them, the most evident one is the explicit objective of the model : the sidelobe level. Depending on the norm used, this level can be estimated by two ways : the L^p-norm sense (the one used in our minimization function), and the infinity-norm sense. Both of them can reveal interesting information. Indeed, even when choosing to minimize according to a particular L^p-norm sense, it is still important to ensure that the signal amplitude will not exceed a given level in particular directions, otherwise the signal coming from these directions could interfere with the signal of interest.

In order to avoid confusion, the sidelobe level term will be understood in its L^p-norm sense when nothing else is mentioned explicitly, as it corresponds to our objective function. However, when comparing the present results with the traditional beamforming

results (usually expressed in the L^∞-norm sense), the reader should be aware that theory demonstrates that the L^p-norm will always be inferior to the L^∞-norm.

Signal to Noise Ratio

Along with the sidelobe level, the Signal to Noise Ratio is another important indicator. The greater the SNR, the less the noise will interfere with the signal of interest. Of course, this ratio depends on a lot of factors, but we are interested in the contribution of the weights in that ratio, as choosing these weights in a smart way can help improve the SNR.

To do so, we are going to develop an explicit expression of the SNR in terms of the weights. Later, this will enable us to compare our actual weights with some ideal weights maximizing this SNR expression. Throughout the reasoning developed below, we are going to work with real constant weights for clarity reasons, but the same kind of reasoning could be applied by extension for complex weights.

The SNR is defined as the ratio between the useful power, which is the signal power in the main direction, and the total power of the noise generated by the antennas. The useful power can be expressed, by definition, as :

$$P_{\text{useful}} = |\sum_{i=1}^{n} w_i EEP_i(\theta_0, \phi_0)|^2$$

If we assume for simplicity that the array consists of isotropic antennas isolated from each other (while we know in reality that their interactions cannot be neglected), with the same amplitude level at the observation direction, we deduct the following relationship of proportionality :

$$P_{\text{useful}} \propto |\sum_{i=1}^{n} w_i|^2 \tag{4.1}$$

Concerning the noise power, it is quite difficult in our situation to estimate the exact contributions of the antennas, so we will consider uncorrelated noise sources n_i specific to each antenna. The total (time-averaged) noise power is therefore given by :

$$
\begin{aligned}
P_{\text{noise}} &= < \sum_{i=1}^{n} |w_i n_i|^2 > \\
&= < \sum_{i=1}^{n} \sum_{j=1}^{n} w_i w_j^* n_i n_j^* > \\
&= \sum_{i=1}^{n} \sum_{j=1}^{n} w_i w_j^* < n_i n_j^* >
\end{aligned}
$$

Furthermore assuming that the noise voltages n_i are uncorrelated, the noise power becomes :

$$
\begin{aligned}
P_{\text{noise}} &= \sum_{i=1}^{n} |w_i|^2 < n_i^2 > \\
&= \sum_{i=1}^{n} |w_i|^2 P_{n_i}
\end{aligned}
$$

where P_{n_i} represents the time-averaged power of the noise of antenna i. Finally, if we consider that these averaged power values P_{n_i} are equal for every antenna, we obtain a new relationship of proportionality for the noise power :

$$
P_{\text{noise}} \propto \sum_{i=1}^{n} |w_i|^2 \tag{4.2}
$$

Combining equations 4.1 and 4.2, we finally find that the SNR is proportional to :

$$
SNR \propto \frac{|\sum_{i=1}^{n} w_i|^2}{\sum_{i=1}^{n} |w_i|^2} \tag{4.3}
$$

Even if the exact SNR cannot be computed from this relationship, it enables us to compare our solution with an ideal situation to have an idea of its quality. Indeed, the situation maximizing the SNR expression 4.3 corresponds to the case where all the weights would have the same amplitude (in this case, the SNR would be equal to the number of weights n).

For the rest of this thesis, we will therefore call SNR the ratio between the quantity computed from equation 4.3, and the ideal SNR value n (this ratio will therefore always be included between 0 and 1).

Directivity

The directivity, introduced in chapter 2, is another important way to characterize the array pattern as it determines how much the radiated power is concentrated in the main

direction.

For an antenna whose Poynting vector is equal to $S(\hat{u}_0)$ in the main direction $\hat{u}_0$, the directivity can be seen as the ratio between the power that would be radiated by an isotropic source whose Poynting vector would be equal to $S(\hat{u}_0)$ in every direction, and the actual radiated power.

If we call $d\Omega$ the solid angle of integration, we can therefore write the directivity as :

$$\begin{aligned} D &= \frac{\iint S(\hat{u}_0) d\Omega}{\iint S(\hat{u}) d\Omega} \\ &= \frac{\iint S(\hat{u}_0) \sin(\theta) d\theta d\phi}{\iint S(\hat{u}) \sin(\theta) d\theta d\phi} \end{aligned}$$

For antenna arrays, the directivity can be obtained by replacing the term $S(\hat{u})$ by the array pattern magnitude $|AP(\hat{u})|$ obtained from equation 2.19. In the particular case of our model, we impose the constraint $|AP(\hat{u}_0)| = 1$. Therefore, the directivity becomes :

$$\begin{aligned} D &= \frac{\iint \sin(\theta) d\theta d\phi}{\iint |AP(\hat{u})| \sin(\theta) d\theta d\phi} \\ &= \frac{4\pi}{\iint |AP(\hat{u})| \sin(\theta) d\theta d\phi} \end{aligned}$$

Finally, as we only consider discrete directions of the array pattern, this ratio of integrals can be approximated as the following ratio of sums :

$$D = \frac{\sum_\Omega \sin(\theta)}{\sum_\Omega |AP(\hat{u})| \sin(\theta)} \tag{4.4}$$

Execution time

Finally, the running time of the algorithm should of course always be monitored for evident practical reasons. In the case of the SKA, this time should be kept under a certain value to enable updating the array calibration reasonably frequently. However, in most situations, the computation time will remain sensibly close and this parameter will therefore voluntarily not be mentioned in that case.

4.1.2 Test procedure

Concerning the test procedure itself, a sensitivity analysis will be made for every particular parameter in order to understand the solution behavior according to that parameter. However, it is important to distinguish two different kinds of parameters. Some of them will be have to be chosen arbitrarily by the user (p-norm used, angular discretization step α), while the rest of it will be intrinsic to the problem definition (observation/interference positions, frequency, ...) and therefore imposed by the situation.

In the case of p and the discretization step α, the sensitivity analysis will enable the user to make an informed choice on the ideal values to pick according to the analysis results. For the other parameters, the sensitivity analysis will provide indications on the results that can be expected from the solution.

Of course, it will not be possible to test each parameter on every configuration of all the other parameters. Therefore, for each analysis, we will define a specific situation, and we will run the algorithm several times while varying only the parameter of interest. For each corresponding instance, the relevant indicators will be computed, enabling to draw conclusions on the solution behavior by analyzing the evolution of these indicators.

In almost every situation, the solutions will be computed on 110 MHz patterns. However, a section will be dedicated to the analysis of the solutions obtained for different frequencies patterns.

4.1.3 Software used

The solutions will be computed using the MOSEK software, which supports SOCP. The solver will be called from the MATLAB environment, as MOSEK developed a toolbox working directly from this environment. Further information about the MOSEK solvers and the MATLAB toolbox can be found in the toolbox documentation on their website [21].

4.2 Sensitivity analysis

4.2.1 Discussion on the norm and discretization step to use

As explained above, the parameters p and α are chosen arbitrarily by the user when running the algorithm. This subsection will therefore discuss the elements to take into account in order to make this choice.

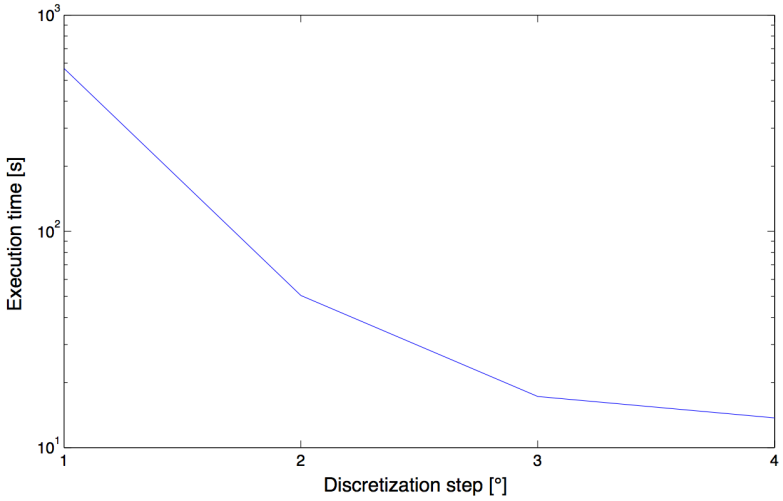

Figure 4.1: Execution times for various values of α for a particular instance

Choice of the angular discretization step α

When looking at our model, we observe that the number of variables increases with complexity $\mathcal{O}(\alpha^{-2})$. Furthermore, the number of second order cones necessary for the modelization is also proportional to α^{-2}. We would therefore expect the amount of time necessary to run the algorithm to follow the same scheme. The graph 4.1 shows the dependency of the execution time of the algorithm with α for a particular instance ($p = 8$, a single interference region of radius equal to 5°).

Given this dependency, the discretization step should not be chosen too small in order to run the algorithm in a reasonable time. However, a certain level of accuracy is still necessary. Otherwise, if the discrete points were too distant, the number of samples would not be sufficient to characterize the signal properly, and the pattern could potentially increase a lot between the discrete points. This is particularly important for the nulling areas, where the pattern is very sensitive and where we want to avoid exceeding the fixed threshold value.

The minimal level of precision can be estimated using by the Shannon-Nyquist sampling theorem [22]. In substance, this theorem states that, for any signal whose frequencies do not exceed a given value B, a sample rate larger than $1/2B$ is sufficient to determine the whole signal entirely and to avoid aliasing while reconstructing it. This result can also be applied to the spatial domain (and similarly angular domain in our case).

Let us get back to the expression of the array radiation pattern (without the mutual coupling effect) :

$$\vec{AP}(\hat{u}) = \sum_{i=1}^{N} w_i \vec{F_0}(\hat{u}) e^{jk\hat{u}\cdot\vec{r_i}} \tag{4.5}$$

with $k = \frac{2\pi}{\lambda}$ the wave number. Recalling that the vector $\hat{u}$ corresponds to the direction of observation :

$$\begin{cases} u = \cos\phi \sin\theta \\ v = \sin\phi \sin\theta \end{cases}$$

the array pattern expression becomes a sum of terms oscillating explicitly with ϕ and θ. In the expression 4.5, the highest "frequency" term corresponds to the case for which r_i is maximal, i.e. $r_i = R$, the radius of the array.

If we apply the Nyquist-Shannon theorem for the angular domain, following the same principle as exposed above for the time domain, we obtain the following Nyquist criterion :

$$\alpha \leq \frac{\lambda}{2R} \tag{4.6}$$

In our case, the SKA-low stations are designed to have a typical diameter of about $35\,m$, which gives us $R \approx 17.5\,m$ [14]. Furthermore, the range of frequencies considered in the case of the SKA-low arrays goes from 50 MHz to 350 MHz, and knowing that the speed of light is equal to $c = 2.998\,10^8 m/s$, we obtain the following wavelength range :

$$\lambda \in [0.857; 5.996]\ m$$

In this range, the worst case scenario (the one minimizing the criterion expression) corresponds to the smallest wavelength. The maximal discretization step for which the signal is totally determined for the entire spectrum is therefore :

$$\alpha \leq \frac{0.857}{35}\ \text{rad} = 1.403^\circ$$

In order to ensure fulfilling the Nyquist criterion for any frequency, the discretization step α should therefore be set to 1° for both θ and ϕ. However, for frequencies under 240 MHz, an angle of 2° will be sufficient. For the rest of this thesis, given the large difference of complexity between the two situations, we will prefer the latter, except when the the problem instances require more precision.

Of course, the same reasoning could be applied for any other set of frequencies or radius.

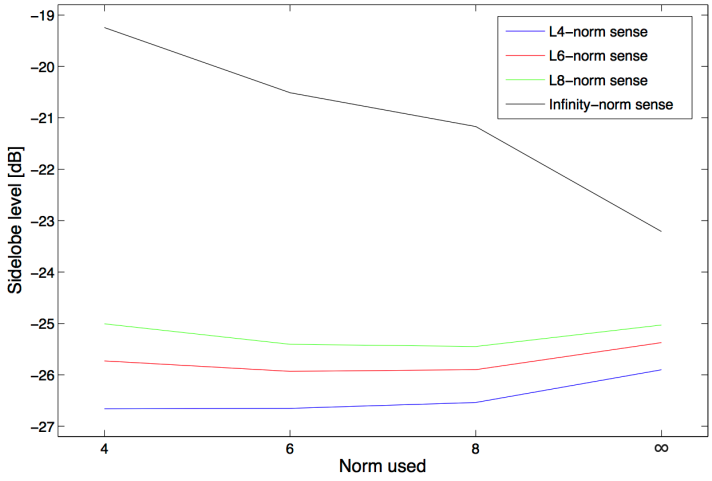

Figure 4.2: Evolution of the solutions norms with p

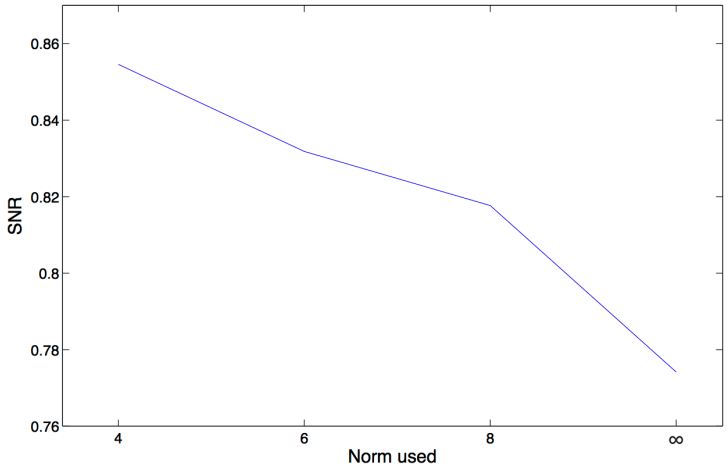

Norm	SNR
L^4-norm	0.8546
L^6-norm	0.8318
L^8-norm	0.8177
L^∞-norm	0.7742

Figure 4.3: Evolution of the solutions SNR with p

Choice of the norm

The type of norm used in the minimization function is another user-based choice that has to be discussed, as it will significantly impact the solution properties. In our context, we consider the set of L^p-norms for any rational p, as well as the particular L^∞-norm (in that case, the model used will be the one developed by Valentin Hamaide mentioned earlier). The graphs 4.2, 4.3 and 4.4 show the behavior of the solutions according to the norm used. In each graph, the x-axis represents the type of norm used to obtain the solution (for $p = 4,6,8$ and the infinity norm). The first graph displays the level of the four different norms for each solution (each solution will of course minimize the corresponding norm), while the second and the third graphs evaluate the SNR and the directivity respectively.

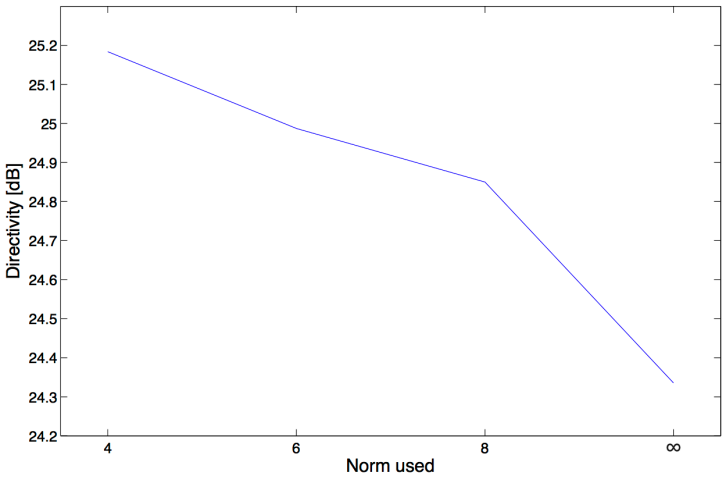

Norm	Directivity
L^4-norm	25.1837
L^6-norm	24.9847
L^8-norm	24.8498
L^∞-norm	24.3356

Figure 4.4: Evolution of the solutions directivity with p

Some interesting behaviors can be deducted from these graphs : while every solution obviously minimizes its own norm, we can observe that the L^∞-norm decreases significantly with p, while the other norms do not show that much variation, except a noticeable increase for the last solution for all three norms.

Furthermore, the SNR and the directivity decrease continuously with p. In the case of the directivity, this result is quite intuitive as, recalling its definition :

$$D(\hat{u}) = 4\pi R^2 \frac{S(\hat{u})}{P_r} \tag{4.7}$$

its denominator (the total radiated power) is very similar to the sidelobe expression in the L^2-norm sense (except that it additionally contains the main lobe region). Therefore, as the value of p gets closer to 2, the directivity increases consequently. For the SNR, the reasoning is not as straightforward, as its denominator can rather be seen as the L^2-norm of the weights vector. However, we can observe by comparing the two graphs that the SNR and the directivity are somehow correlated.

Furthermore, it is interesting to note that the execution times are quite similar in all situations, with a small increase for $p = 6$.

Considering all these aspects, the choice of p should thus be large enough to prevent too large peaks outside the main region, but this choice should also be small enough to keep higher SNR and directivity values. The final value will be left to the user discretion, but for the rest of this thesis the value $p = 8$ will be used for the tests, if not mentioned otherwise.

Finally, in order to visualize clearly the differences between the norms used, the graphs 4.5 and 4.6 compare the patterns of the L^4-norm solution and the L^∞-norm solution, for

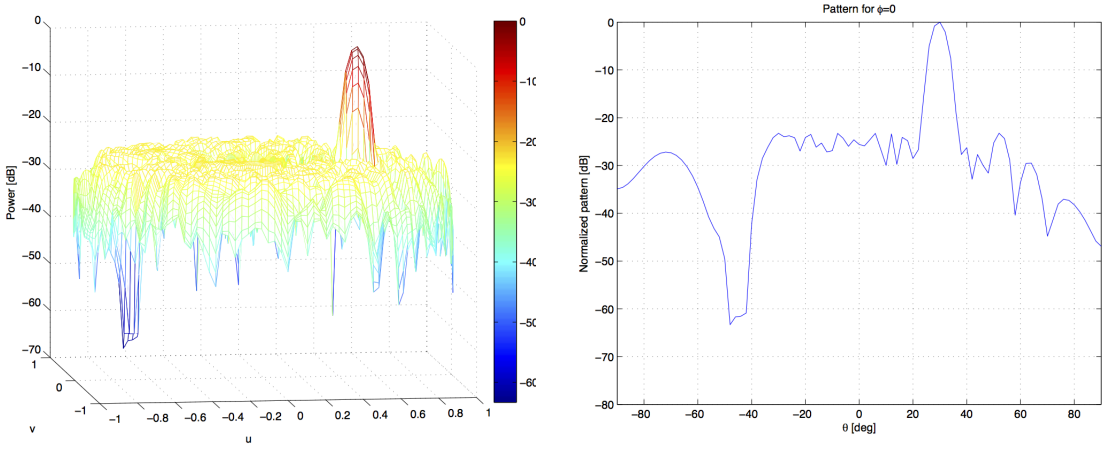

Figure 4.5: Solution obtained from the L^{∞}-norm minimization

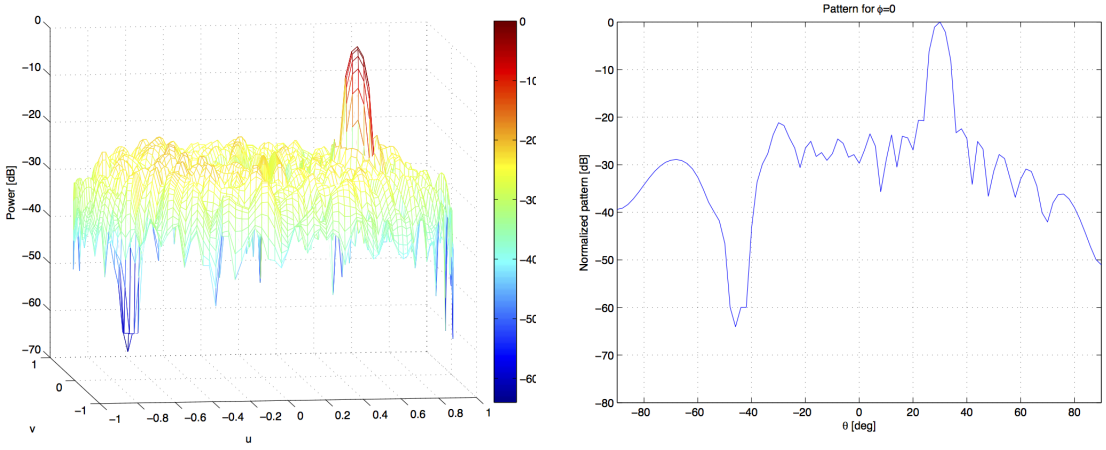

Figure 4.6: Solution obtained from the L^{4}-norm minimization

a particular instance. As expected, we can observe that the L^4-norm allows the maximal value of the L^{∞}-norm to be exceeded in some points, for a globally lower average sidelobe level.

4.2.2 Main lobe characteristics

In this part, we are going to quantify the effect of the main lobe parameters, in the absence of interference. We will start by computing the solution indicators for various observation directions (θ_0, ϕ_0) to see the respective effects of the two coordinates, for a constant main lobe radius equal to 5° at half power level. We will then vary the value of this beam width to study its effect on the solution.

Main lobe position

The graphs of figure 4.7 show the dependency of the sidelobe level (L^8-norm sense) with θ and ϕ respectively. In order to get situation-neutral results, we ran the algorithms several times for main directions distributed on the whole domain (more precisely, we varied θ from 0° to 90° with 15° increments, and ϕ from 0° to 360° with 45° increments). We then regrouped the corresponding solutions angle by angle, and took the average values for each case.

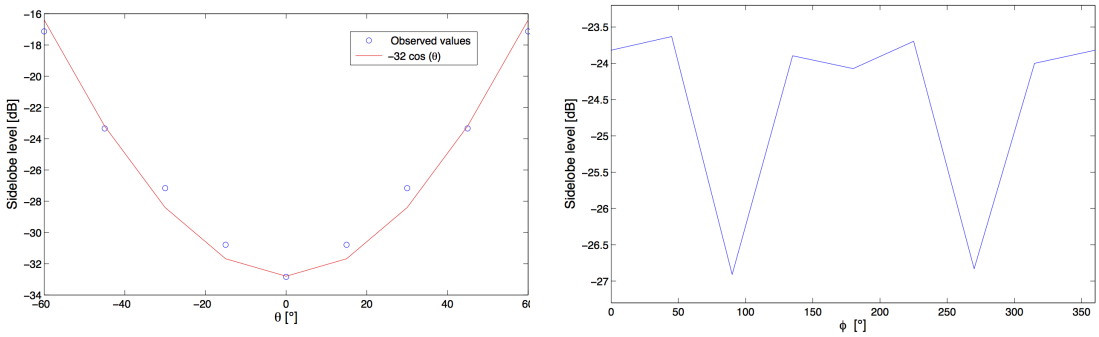

Figure 4.7: Sidelobe level for various main lobe directions (averaged values)

Concerning the θ dependency, we can first remark that the sidelobe level is minimal in the vertical direction ($\theta = 0$), where it is inferior to -30 dB. When moving away from the vertical, the sidelobe level increases significantly with θ, approximately following a $\cos(\theta)$ dependency.

For values of θ above 60°, the algorithm returns in some cases an "exit" status stating that the solution optimality is not ensured anymore. We will see later that this kind of issue will also appear in other situations, mostly due to numerical instabilities of the solver when large values of p are involved (indeed, the objective function contains variables to the p^{th} power, possibly resulting in huge or similarly very small values). One way to improve this situation will be to rescale the variables before running the algorithm, and then divide them by the same scaling factor after the solution is obtained.

The solution dependency with the ϕ_0 angle of the main direction, however, is less clear. In most directions, the sidelobe level stays constant with ϕ, with an average value around -24 dB, except when the source is around $\phi = 90°$ (or similarly in the opposite direction, $\phi = 270°$). In that particular situation, the sidelobe level reaches about -27 dB, which represents a non-negligible difference of 3 supplementary dB.

Main lobe width

In order to analyze the algorithm sensitivity with respect to the main lobe width, one possibility is to increase the size of the main region, not concerned by the sidelobe minimization

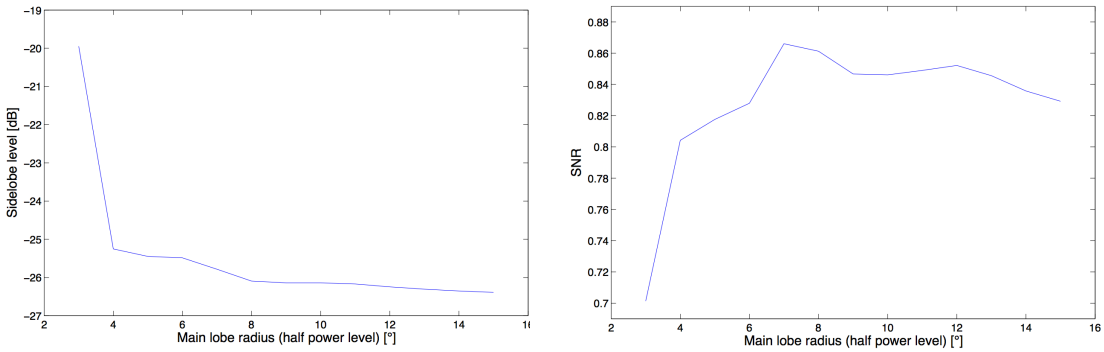

Figure 4.8: Solution behavior with to the main region size

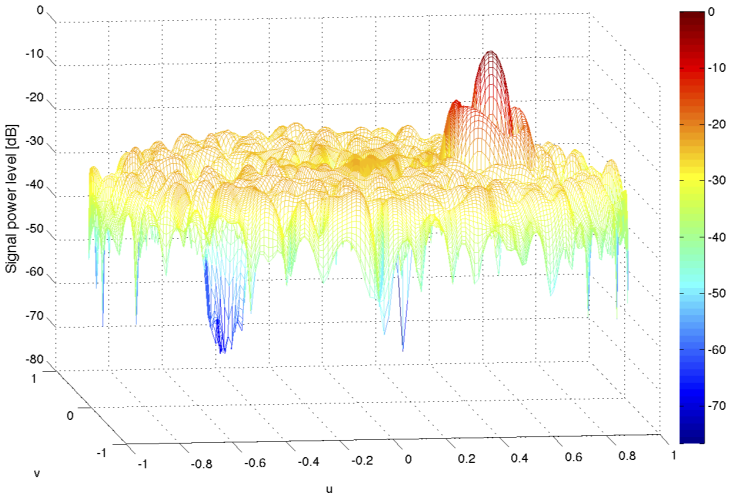

Figure 4.9: Large Width

function. Indeed, as the sidelobe level typically has the tendency to decrease when the main lobe width increases, enabling a larger main lobe radius while still minimizing the sidelobe level should result in an effectively larger main lobe.

The graphs of figure 4.8 show the SLL and SNR dependency with the main lobe radius r_0 (ranging from 3° to 15°) for a particular instance. We can observe a important drop of 5 dB of the sidelobe level between radiuses of 3° and 4°, while for larger radiuses, the SLL decreases more slightly, losing one supplementary dB between 4° and 15°. Similarly, the SNR increases steeply in the first iterations and stabilizes around 0.85, with small variations of this value.

At first sight, these results follow the principle stated above. However, while looking closer to the solution, we remark that, for values of r_0 above 6°, the algorithm has tendency to converge to optimal solutions for which the main lobe width stays relatively constant but where the first sidelobes (now in the main region) are amplified, instead of effectively increasing the main lobe width. An example of this phenomenon is shown on fig 4.9.

One possibility to tackle this problem would be to force the signal to stay above the half-power level inside the whole region defined by the desired radius. However, as explained above while building the model, imposing lower bounds on the signal level is not convex, and it would therefore be very difficult to impose such a condition without losing the model convexity.

4.2.3 Interference characteristics

In this section, a comprehensive sensitivity analysis of the interference characteristics (number of interference sources, position and width of theses sources, and imposed cancellation level) will be performed.

Before going further, it is important to note that the solution is heavily constrained by the signal cancellation imposed in the interference regions (especially for critical situations, when the interference sources are located very close to the main direction, or when the cancellation level is very deep). As these nulling constraints are applied only on discrete directions of the interference region, we could potentially observe an important increase between these discrete directions and it is therefore important to inspect the signal everywhere in the region.

As a general consideration, two solutions can be envisaged if we notice a too important increase : either increasing the density of discrete directions concerned by the cancellation constraint (preferably not in the whole domain to avoid increasing the execution time too much), or imposing a deeper cancellation level, to be sure that the signal will stay under the initial level even between the discrete points.

Number of interference sources

In the first instance, let us analyze how the solution behaves when imposing the cancellation of one or more interference regions. The graphs of figure 4.10 show the contribution of the number of such sources on the sidelobe level and the SNR, respectively. For this analysis, the main direction was placed at $\theta = 30°$, and interference regions of radius equal to 5° were added one by one on various directions, ensuring that they were not too close to each other or from the main direction to avoid proximity effects.

We can clearly observe a continuous increase of the SLL with the number of sources n to be cancelled. This relation seems linear, with an increment about 0.5 dB for each interference source added. We can also remark a global decrease of the SNR with n, with a total loss of about 10% of the initial SNR value when adding 5 sources.

For the next parameters, we are now going to focus on the case of a single interference source.

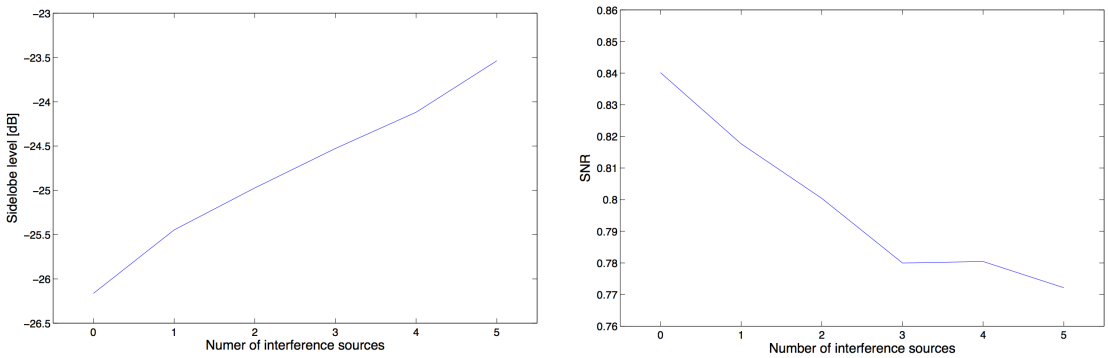

Figure 4.10: Solution behavior with the number of interference sources

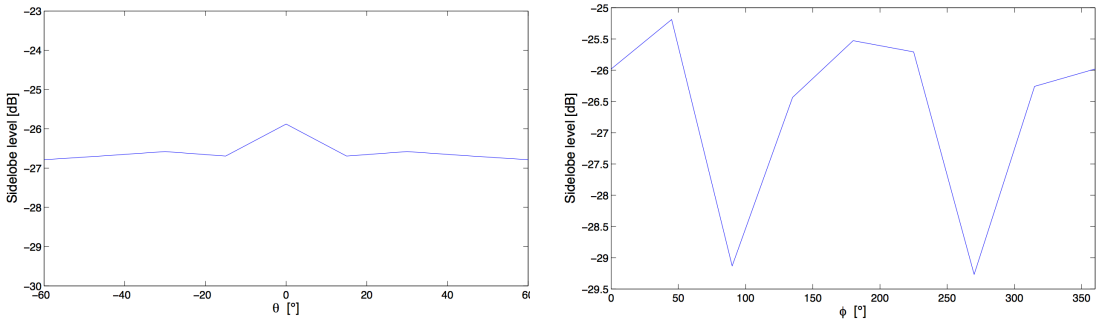

Figure 4.11: Sidelobe level according to the interference direction

Absolute interference direction

Concerning the direction from which the interference is emitting, we will split the analysis into two separate parts. In this subsection, we will consider the absolute location in the domain Ω, assuming that it is sufficiently far from the main direction. Then, we will observe how the solution reacts when progressively bringing the interference and observation directions closer, independently from their absolute values.

In order to analyze the absolute direction effect, we will repeat the same process as we did for the main lobe direction (θ_0, ϕ_0), this time for the interference direction (θ_1, ϕ_1). In each situation, the main lobe will be located in the opposite direction $(\theta_1, \phi_1 + 180°)$. The results are displayed on graph 4.11.

Unlike the main lobe, the absolute θ-direction of the null does not seem to have a significant effect on the solution. The averaged sidelobe level remains constant at about -27 dB, with only a small increase (barely 1 dB) for $\theta = 0°$.

For the ϕ-direction however, the situation is quite similar to the case of the main lobe : while the average sidelobe level remains constant for most azimuthal directions (at about -26 dB), we observe a clear drop of 3 dB in the $\phi = 90°$ direction, and similarly in

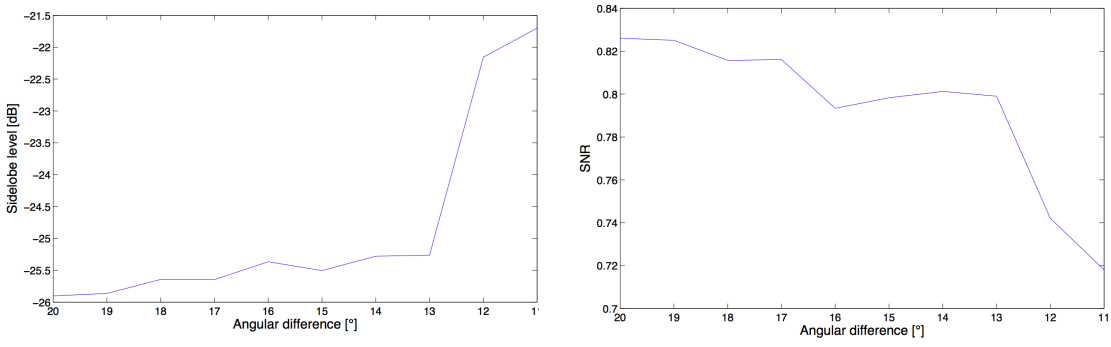

Figure 4.12: Solution behavior with the distance to the source

the opposite $\phi = 270°$ direction. One hypothesis to explain this phenomenon could be the fact that this direction would be related to the antennas reference direction.

Relative interference direction

In order to understand the effect of the proximity between the interference and observation directions, an interference source will be placed at a 20° distance from the main lobe, and this gap will progressively be reduced degree by degree. During this process, both the interference region and the main lobe will have a radius equal to 5°. The resulting SLL and SNR evolutions with respect to the relative distance are shown on fig. 4.12.

When the distance stays sufficiently high, it does not impact the solution too much as we can only observe a slight increase of the SLL and a slight increase of the SNR when closing the gap, but still in the same order of magnitude. However, there seems to be a critical distance under which the solution appears to deteriorate. In our case, this distance is approximately equal to 10°, which corresponds to the sum of the interference and main lobe radiuses. In other words, the situation becomes critical when the interference region intersects the main lobe.

When the distance gets close to that critical 10° value, the sidelobe level brutally increases by 3 dB, and the SNR similarly undergoes a big drop. For distances under 10°, it becomes even impossible for the algorithm to find an optimal solution. In this particular situation however, this appears to be due to the absence of feasible solution rather than the numerical instabilities mentioned above.

When the observation and interference directions are this close, it is furthermore important to ensure that the signal level does not overly exceed the imposed cancellation level between the discrete directions where the constraints are applied. To this end, the signal levels between these directions were checked at each iteration, and the corresponding maximal level values of each iteration can be found on graph 4.13.

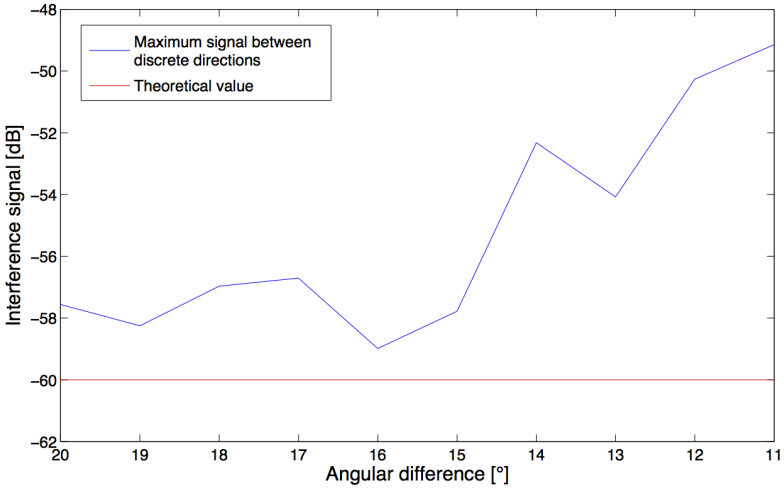

Figure 4.13: Maximal level between the constrained discrete directions

While the theoretical value of 60 dB is not exceeded by more than a few dB for distances above 15°, we observe an important increase for smaller gaps, until 10 dB higher than the required level in the worst case, near the critical distance of 10°. This distance therefore seems to be a "feasibility barrier" for the solution. This can be explained by the fact that the angular size of the main lobe is dependent on the signal frequency and the array diameter. When the interference region intersects the main lobe region, the distance becomes insufficient to allow a main lobe large enough to obtain a feasible solution.

Interference size

In this part, we are going to gradually increase the radius of the cancellation region, in order to observe its specific influence on the solution.

Before analyzing the results, a small precaution is necessary. In our model, the constraints are applied over discrete directions only. Concerning the signal cancellation constraint, one should therefore ensure that the number of such discrete directions is sufficiently large to cover the interference area correctly. To ensure respecting this, a condition could be set on the discretization step α and the radius r of the interference region (this condition will of course work in pair with the Nyquist criterion mentioned above). In our case, we will use :

$$\frac{r}{\alpha} \geq 2 \tag{4.8}$$

This way, we ensure that the total number of points is always sufficient to cover a sufficiently large part of the cancellation area. As we chose to use the discretization step $\alpha = 2°$, we will therefore start our analysis with interference regions of radius equal to 4°.

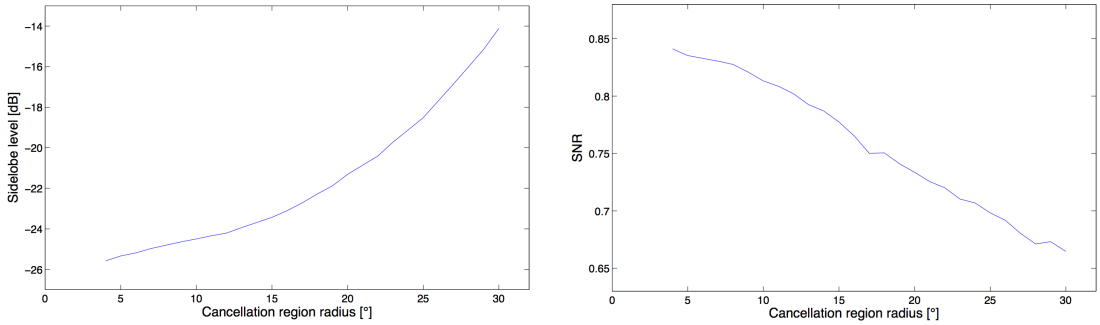

Figure 4.14: Solution behavior with the interference region size

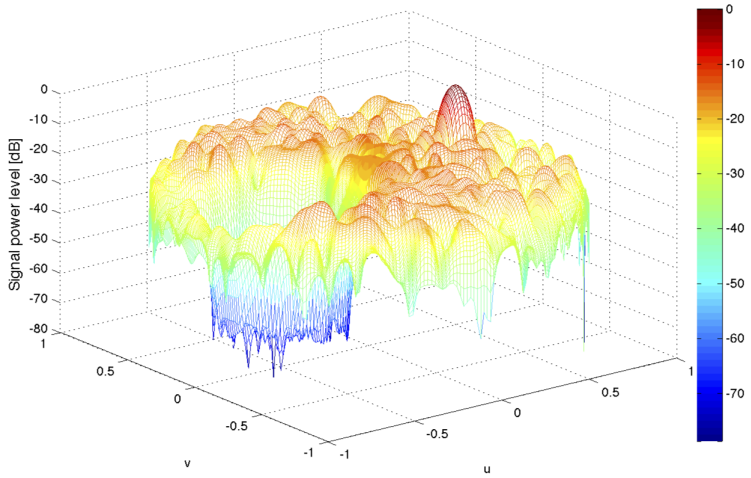

Figure 4.15: Example of solution with very large interference region

Figure 4.14 shows the effect of the interference radius on the SLL and SNR. We observe that the sidelobe level seems to grow exponentially with r. In fact, this increase seems to be proportional to the region surface, and therefore to r^2.

Despite this dependency, the magnitude of this increase is not too important, with only a 10 dB gain between interference regions of 3° radius and 25° radius. This outlines the fact that this method is particularly well suited when the cancellation of very large regions is required. The graph 4.15 displays an example of situation involving a interference region of radius 25°.

This apparently slow decrease of the SLL, however, should be tempered by the fact that, for large values of r, the SLL is significantly influenced by the large part of the domain concerned by the cancellation constraint, therefore reducing the average signal level as it included in its computation.

Concerning the SNR, the graph of figure 4.14 outlines a linear decrease with the radius

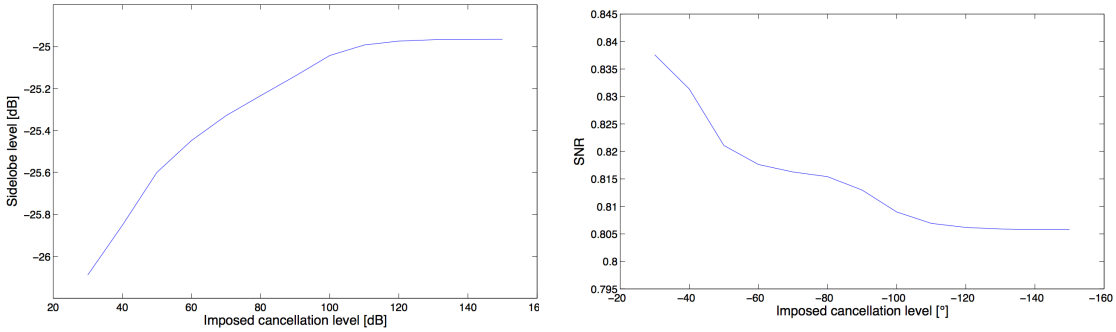

Figure 4.16: Solution behavior with the imposed cancellation level

r, but its value stays once again reasonable even for large radiuses (0.7 for $r = 25$). All these considerations hold only when the cancellation region remains sufficiently far from the main direction.

Cancellation level

The last analysis of this section dedicated to the nulling characteristics concerns the level at which the signal is constrained in the interference region. Once again, we are going to vary the cancellation level L for a specific instance, starting with a low constraining value (-30 dB, just under the average sidelobe level), and decreasing gradually to reach higher values. The graph 4.16 shows the sidelobe level variation with respect to the level limitation.

For shallow cancellation levels, the sidelobe level increases significantly with L. However, when approaching deeper levels (around -100 dB), the SLL seems to stabilize around -25 dB. The SNR follows the same tendency, with a steep decrease at the beginning, and stabilizing around 0.805 for higher values of L.

It is particularly crucial in this case to control the signal level outside the discrete constrained points. Indeed, there is no point deepening further the signal level on the discrete points, if the signal level does not decrease similarly around these points. We can observe on the blue curve of graph 4.17 that, for values above -80 dB, the maximal level does not follow the expected level and stabilizes at about -78 dB, which seems to be the minimal achievable level in this precise situation. However, it is important to keep in mind that the element patterns cannot be known perfectly, and requiring further precision would therefore not especially be useful in practical.

We can also observe on the green curve that, even on the discrete directions, the algorithm cannot reach level values below -140 dB (in that case however, the ratio between the maximal and interference levels becomes really large, and this issue is probably due to the limited machine precision).

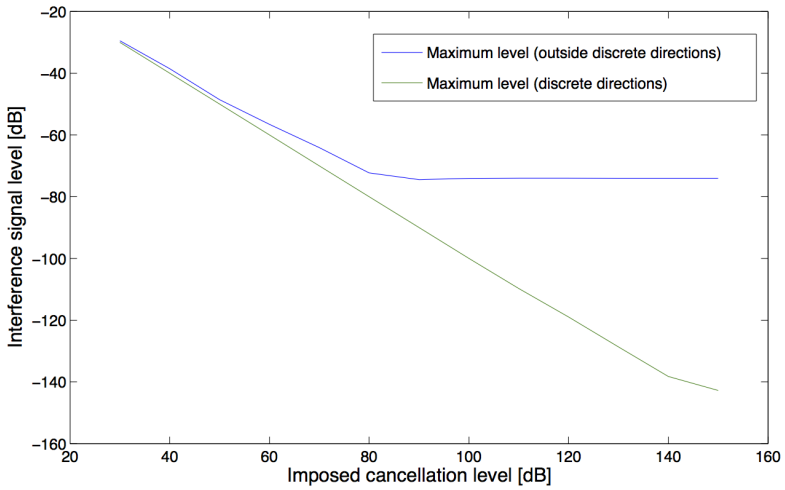

Figure 4.17: Maximal level in the interference region, for various cancellation levels

4.2.4 Frequencies

Until now, all the solutions were computed on patterns obtained for a frequency equal to 110 MHz. This section will therefore be dedicated to the comparison of solutions obtained for other frequencies patterns.

Before running the algorithm on different instances, we should be careful to the fact that modifying the frequency will also modify significantly the patterns characteristics. Therefore, it is important to adapt the algorithm parameters accordingly :

- For lower frequencies, the width of the pattern lobes will increase significantly. It might therefore be necessary to allow a larger main lobe radius, otherwise the main region Ω_0 could not be sufficient to contain the entire main lobe anymore.
- Conversely, when increasing the frequency, the distance between the lobes decreases accordingly, and the discretization step α should therefore be reduced accordingly, to avoid violating the Nyquist criterion

The solutions obtained for frequencies of 50 MHz and 200 MHz (with appropriate algorithm parameters) are shown on figure 4.18. As expected, we can clearly observe an important increase of the lobes widths with the frequency.

The figure 4.19 shows the variations in terms of SNR and SLL of the optimal solutions for three different frequencies (50 MHz, 110 MHz and 200 MHz respectively). This table outlines an important deterioration of the SLL when increasing the frequency (around -27 dB for 50 MHz, above -22 dB for 200 MHz). However, concerning the SNR, we can observe

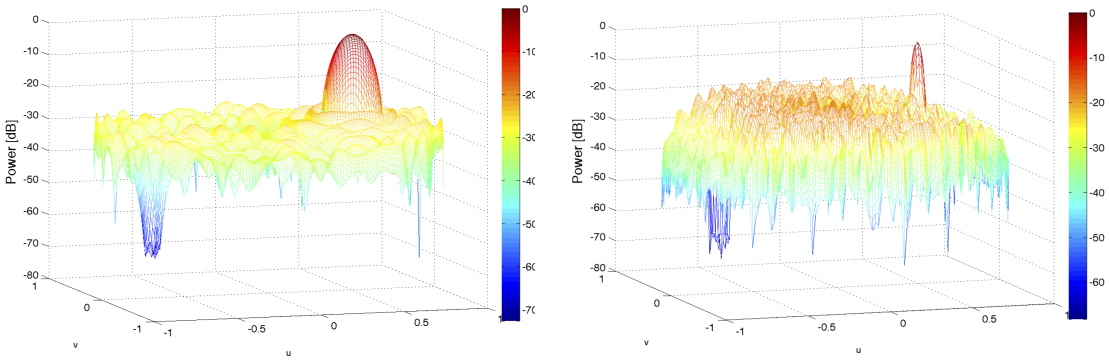

Figure 4.18: Solution examples for 50 MHz and 200 MHz patterns respectively

Frequency	SLL [dB]	SNR
50 MHz	-27.0481	0.6900
110 MHz	-25.4479	0.8177
200 MHz	-21.6762	0.8536

Figure 4.19: Comparison between solutions obtained for patterns of different frequencies

the opposite effect, with a significant decrease with the frequency (0.69 for 50 MHz, 0.85 for 200 MHz).

When analyzing these results, it is of course important to keep in mind that these solutions were computed with slightly different parameters, as explained above.

4.2.5 Global results discussion

Several crucial conclusions can be drawn from the previous considerations. First of all, the L^p-norms enable achieving better SNR and directivity than the L^∞-norm, as well as a lower average signal at the cost of higher values in some particular directions. Depending on the chosen value of p, we can adjust this compromise depending on the required characteristics of the solution.

Furthermore, choosing an α discretization step of 2°, as done in these tests, enables finding an optimal solution in less than 1 minute. While this is slower than the direct methods (finding solutions in almost real time), this duration is still reasonable, and can further be improved with more powerful hardware.

Furthermore, the model proved to be very efficient when dealing with very large sources of interference, even for cancelling the signal of entire parts of the sky.

Concerning the problem-intrinsic parameters, some of them seem to have a higher impact on the solution than others. This is particularly true for the θ-coordinate of the main lobe direction, the distance between this main lobe and the interference sources, as

well as the cancellation level. For these parameters, the algorithm was sometimes not able to find an optimal solution for the most constraining values.

In most cases however, the numerical problems seem to be due to the algorithm implementation and to the solver rather than resulting from the model itself. Indeed, for some particular instances, the sidelobe level and other indicators of the solution were still decent when pushing the parameters, but a few constraints were suddenly violated while the solution was still considered optimal by the solver.

These numerical instabilities could be due to the fact that high powers are involved in the objective function (in the case of these tests, this function was a sum of variables to the eighth power). To avoid the negative effects, it was necessary to rescale the variables before introducing them in the algorithm. However, in the case $p = 8$, the range of effective scaling factors was very restrictive and sometimes even had to be adjusted depending on the parameters used. The scaling choice was even made more difficult by the fact that these numerical problems were not detected by the solver, as the solutions were considered optimal in that case.

To improve this issue, some solutions could be imagined, as doing an automatic rescaling of more variables, or avoiding too large values of p for the critical situations.

4.3 Robustness

After having analyzed the model sensitivity with respect to the different parameters, it is important to determine to which extent the solution properties would be preserved when adding some uncertainty to the computed optimal weights. This property is called robustness.

To do so, we will apply random perturbations to the weights, and compute the perturbed pattern corresponding to those new weights. We will then compare the perturbed solution with the initial one, in terms of SLL and SNR. In order to cancel out the randomization effects, we will repeat this process a certain number of times, and average the results. The perturbation will consist in a random normally distributed vector, with zero mean and a standard deviation equal to 10% of the average magnitude of the weights.

As the interference region is a particularly critical area, the whole process will be repeated for different cancellation levels (-40 dB, -60 dB and -80 dB), and the signal level in the interference region will also be analyzed in each case.

The results obtained for the different situations can be found below. The tables of figure 4.20 show the differences between the initial and the perturbed solutions, in terms of sidelobe level and signal to noise ratio. We can observe that, regardless of the cancellation level, the SLL and SNR stay very similar after the weights perturbation. For the SLL, we

	Initial	Perturbed (avg.)
-40dB	-25.8523	-25.6866
-60dB	-25.4479	-25.2851
-80dB	-25.2338	-25.0931

(a) Sidelobe level comparison

	Initial	Perturbed (avg.)
-40dB	0.8314	0.8273
-60dB	0.8176	0.8144
-80dB	0.8154	0.8135

(b) SNR comparison

Figure 4.20: Comparison between the initial and perturbed solutions for different cancellation levels

Target	Maximal	Mean
-40dB	-36.7075	-40.3444
-60dB	-41.5959	-47.0555
-80dB	-42.2758	-47.9196

Figure 4.21: Maximal and mean signal levels in the interference region

remark a small average increase of about 0.2 dB in every case, while the SNR is subject to a decrease between 0.2% and 0.4% depending on the situation.

For the signal level in the cancellation area however, the variations (displayed on figure 4.21) are way more significant. In the case of an imposed cancellation level of -40 dB, the average signal stays in the required level with a maximum value only 4 dB over the limit. For the 60 dB and 80 dB limitations however, this is not the case anymore. In both situations, the average signal in the interference cannot go lower that -47 dB, with a maximum value around -42 dB. These values therefore seem to be a limit of the achievable cancellation level after perturbation in our case, whatever the cancellation level initially achieved by the algorithm.

The same process was also repeated for different perturbation magnitudes. For 5% perturbations, we obtained an achievable average level of about -52 db, for a maximal level of -47 dB. Similarly, for 20% perturbations, we obtained an average level of -36 dB, and a maximal level of -40 dB. We can therefore see that the cancellation level is significantly impacted by the magnitude of the perturbations.

In order to have a visual representation of the way the solution is affected by the perturbations, an example is shown on figures 4.22 and 4.23, for an initial cancellation level of -60 dB.

Some possibilities exist to improve the robustness of the solution to the weights uncertainty [23][24]. In order to rigorously ensure that the constraints would be satisfied for any weights perturbation of a given amplitude, we can perform an analysis of the worst case scenario for the weights, and then adapt the model consequently. However, by studying carefully the problem structure, we can deduct that it would require to solve an auxiliary model that could not be formulated as a convex problem. This approach will therefore

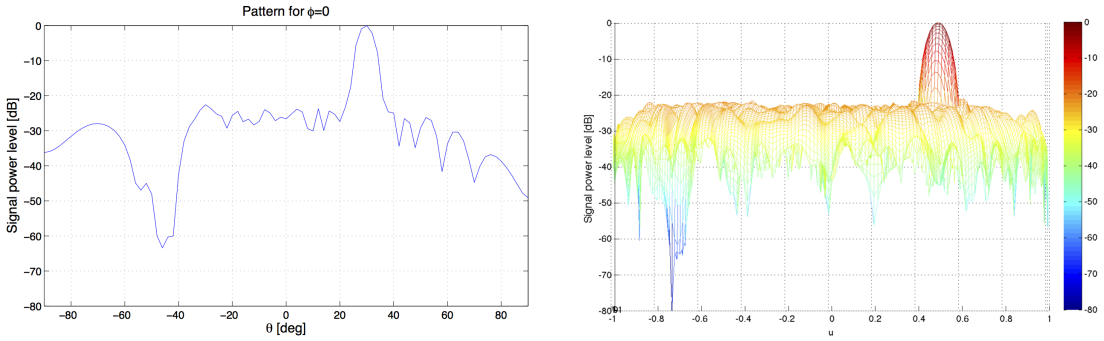

Figure 4.22: Solution before perturbation

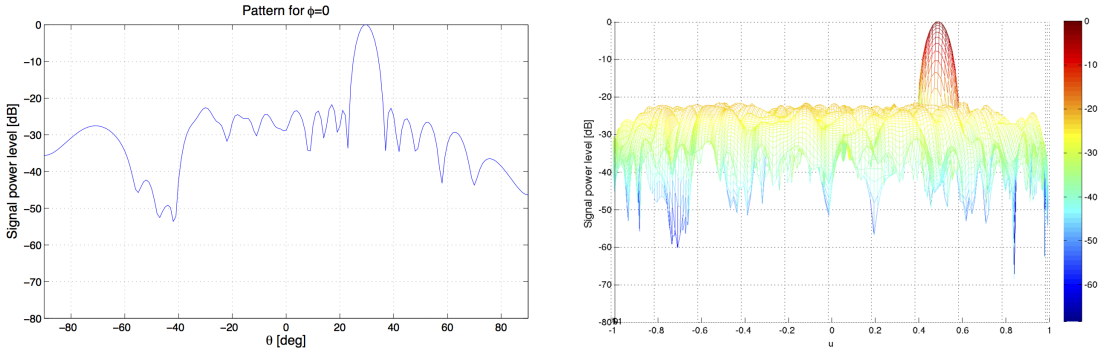

Figure 4.23: Solution after perturbation

not be studied here.

It is also sometimes suspected that adding a regularization term for some variables in the objective will have a positive effect on the robustness of the model to these variables. In our case, this can be modeled in a convenient way, without losing the model convexity. More precisely, taking back our minimization expression :

$$\text{minimize} \sum_{\Omega \setminus \Omega_0} |AP(\theta, \phi)|^p \sin(\theta)$$

we add an additional term proportional to the L^2-norm of the weights vector (Tikhonov regularization). The new function becomes :

$$\text{minimize} \sum_{\Omega \setminus \Omega_0} |AP(\theta, \phi)|^p \sin(\theta) + \lambda \|w\|_2^2 \tag{4.9}$$

This problem can easily be transformed into a second order cone program in the following way :

$$
\begin{array}{lll}
\text{minimize} & t + \lambda s & \\
\text{subject to} & \displaystyle\sum_{i \in \Omega \setminus \Omega_0} y_i \sin(\theta) \leq t & \\
& x_i^2 \leq y_i & \text{on } \Omega \\
& {Z_{H,i}^r}^2 + {Z_{H,i}^{im}}^2 + {Z_{V,i}^r}^2 + Z_{V,i}^{im\,2} \leq x_i & \text{on } \Omega \\
& \displaystyle\sum_{i=1}^{n} w_i^2 \leq s &
\end{array}
$$

where the parameter λ can be chosen arbitrarily be the user. In the next section, as we will develop a model optimizing simultaneously two conjoint objectives, we will obtain a formulation that will coincidentally have this specific shape. We will therefore evaluate the effects of this regularization in the corresponding section.

Chapter 5

Model improvements

5.1 Multi-objective Optimization

Until now, the proposed algorithms focused on a single main objective : minimizing the sidelobe level. However, we saw that another parameter was particularly important in our analyses : the signal to noise ratio. Therefore, one could decide to optimize simultaneously both criteria. This can be achieved through multi-objective optimization.

5.1.1 Introduction to multi-objective optimization

Multi-objective optimization consists in optimizing simultaneously two or more objective functions. A comprehensive survey of the current available techniques and their applications has been made by Marler and Arora in 2003 [25]. Further information can also be found in [26].

We can divide the existing techniques into three main categories. The first one contains the *a priori* methods, in which the relative importance of the different objectives is determined in advance before running the algorithm, and these methods therefore generate a single optimal solution. On the other hand, the *a posteriori* methods generate a set of potential solutions, among which the user can select the optimal one depending on the set characteristics. Finally, the last class contains all the methods for which no preference criteria are required. In the context of this thesis, we will focus on the *a posteriori* methods, in order to let the final choice to the algorithm user.

Before anything, let us introduce a few concepts necessary to characterize the solutions obtained from multi-objective programs. Let us consider the set $\mathbf{X}$ of the attainable solutions for a particular problem. For each solution $\mathbf{x} \in \mathbf{X}$, we associate the n cost functions $\mathbf{F}(\mathbf{x}) = [F_1(\mathbf{x})\ F_2(\mathbf{x})\ ...\ F_n(\mathbf{x})]$ that we wish to minimize jointly.

Definition 5.1 *A feasible solution* $\boldsymbol{x}^* \in \boldsymbol{X}$ *is* ***Pareto Optimal*** *iff there is no solution*

$$\boldsymbol{x} \in \boldsymbol{X} \text{ such that } \begin{cases} \boldsymbol{F}(\boldsymbol{x}) \leq \boldsymbol{F}(\boldsymbol{x}^*) \\ F_i(\boldsymbol{x}) < F_i(\boldsymbol{x}^*) \quad \text{for at least one } i \end{cases}$$

This definition means that a solution $\mathbf{x}$ is Pareto-optimal if and only if it is not possible to improve any of the objectives without deteriorating others. Their exists a weaker version of this property called weak Pareto-optimality :

Definition 5.2 *A feasible solution $\boldsymbol{x}^* \in \boldsymbol{X}$ is **weakly Pareto Optimal** iff there is no solution $\boldsymbol{x}^* \in \boldsymbol{X}$ such that $\boldsymbol{F}(\boldsymbol{x}) < \boldsymbol{F}(\boldsymbol{x}^*)$*

which means that it is not possible to improve all the objectives simultaneously.

The method chosen for our algorithm will be the weighted sum method, which is one of the most common multi-objective methods. It simply consists in minimizing a weighted sum of all the objectives F_i :

$$\text{minimize } U(\mathbf{x}) = \sum_i \lambda_i F_i(\mathbf{x}) \tag{5.1}$$

where the parameters λ_i are chosen arbitrarily by the user and will define the preferences between the cost functions. The optimality conditions for this method will be discussed below. When applied with a particular set of weights λ_i, this method is part of the *a priori* category. However, we will launch various iterations of this method for various weights values, ensuring that the set of solutions obtained represents the entire Pareto-optimal set, i.e. the set of all the Pareto-optimal solutions. This process can therefore be considered as an *a posteriori* method.

5.1.2 Multi-objective model

In our case, we will consider two objectives : the sidelobe minimization, which was the primary goal all along this thesis, and the SNR maximization. Some multi-objective models have already been developed in beamforming (for instance, see [27]), but not with the the same criteria. While the formulation of the first objective has been discussed largely, the way to formulate the second while keeping the conicity of the model is less obvious.

Let us recall once again the SNR definition :

$$SNR = \frac{P_{\text{useful}}}{P_{\text{noise}}}$$

In our model, we imposed the signal power density in the main direction to be equal to unity (the important part here is the fact that it is constrained to a given level, rather than the level value itself). Therefore, minimizing the noise power P_{noise} while keeping the useful power P_{useful} constant amounts to maximimize the SNR.

Furthermore, we showed on last section (equation 4.2) that the noise power was proportional to the sum of the squared amplitudes of the weights :

$$P_{\text{noise}} \propto \sum_{i=1}^{n} |w_i|^2$$

Therefore, maximizing the SNR can be achieved through the following objective :

$$\text{minimize} \sum_{i=1}^{n} |w_i|^2 = \sum_{i=1}^{n} {w_i^{re}}^2 + {w_i^{im}}^2 \tag{5.2}$$

As this function is a sum of squared terms, it can easily be formulated as a second-order cone program :

$$\begin{array}{ll} \text{minimize} & s \\ \text{subject to} & \displaystyle\sum_{i=1}^{n} {w_i^{re}}^2 + {w_i^{im}}^2 \leq s \end{array}$$

Combining our initial model with this new program can therefore be done by combining the two objective functions as done in equation 5.1. The resulting model, for $p = 4$ and arbitrary parameters λ_1 and λ_2 can be found below.

$$\begin{array}{lll} \text{minimize} & \lambda_1 s + \lambda_2 t & \\ \text{subject to} & \displaystyle\sum_{i=1}^{n} {w_i^{re}}^2 + {w_i^{im}}^2 \leq s & \\ & \displaystyle\sum_{i \in \Omega \backslash \Omega_0} y_i \leq t & \\ & x_i^2 \leq y_i & \text{on } \Omega \\ & {Z_{H,i}^r}^2 + {Z_{H,i}^{im}}^2 + {Z_{V,i}^r}^2 + {Z_{V,i}^{im}}^2 \leq x_i & \text{on } \Omega \\ & Z_H^r = \mathbf{P}_H^r \mathbf{w}^r - \mathbf{P}_H^{im} \mathbf{w}^{im} & \text{on } \Omega \\ & Z_H^{im} = \mathbf{P}_H^r \mathbf{w}^{im} + \mathbf{P}_H^{im} \mathbf{w}^r & \text{on } \Omega \\ & Z_V^r = \mathbf{P}_V^r \mathbf{w}^r - \mathbf{P}_V^{im} \mathbf{w}^{im} & \text{on } \Omega \\ & Z_V^{im} = \mathbf{P}_V^r \mathbf{w}^{im} + \mathbf{P}_V^{im} \mathbf{w}^r & \text{on } \Omega \\ & \mathbf{P}_{co}^r \cdot \mathbf{w}^r - \mathbf{P}_{co}^{im} \cdot \mathbf{w}^{im} = 1 & \text{for } (\theta_0, \phi_0) \\ & \mathbf{P}_{co}^r \cdot \mathbf{w}^{im} + \mathbf{P}_{co}^{im} \cdot \mathbf{w}^r = 0 & \text{for } (\theta_0, \phi_0) \\ & x_i \leq C^2 & \text{on } \Omega_i \\ & x_i \leq 1 & \text{on } \Omega_0 \\ & x_i \leq 0.5 & \text{on } \Omega_{hp} \backslash \Omega_0 \end{array}$$

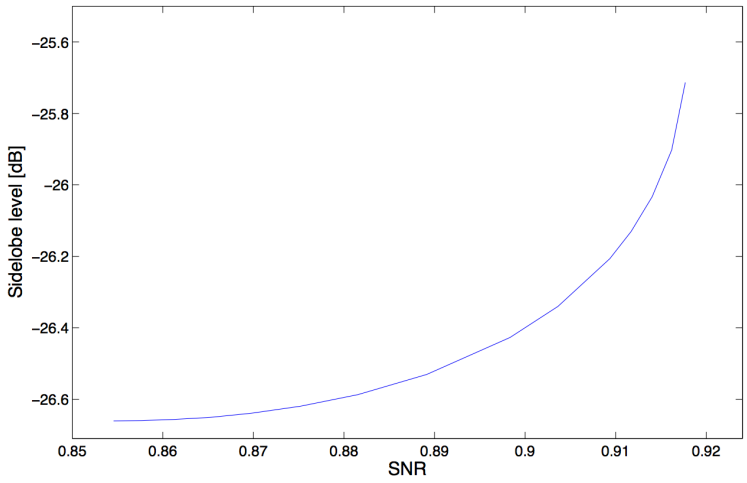

Figure 5.1: Trade-off curve between the SNR and the SLL

Without loss of generality, we will choose $\lambda_2 = 1 - \lambda_1$. However, in order for the two coefficients to have the same relative importance on the objective, we will divide them by the optimal value of their respective objectives functions. We will furthermore impose $\lambda_1, \lambda_2 \geq 0$.

5.1.3 Results analysis

The trade-off curve between the SLL and the SNR depending on the value of λ_1 is displayed on the graph 5.1. We can observe that a significant SNR can be achieved with this method without deteriorating too much the sidelobe level, especially for low values of λ_1. For example, for $\lambda_1 0.3$, it is possible to increase the SNR by about 5%, while increasing the sidelobe level (in the L^4-norm sense) by less than 1%. Of course, the final choice of the optimal λ_1 value will be left to the user.

Let us now discuss the optimality conditions relative to this model, to ensure that the Pareto curve presented above represents correctly the entire Pareto-optimal set. It can be proven that, for any $\lambda_i \geq 0$, the weighted sum method will always yield Pareto-optimal solutions. However, we still need to prove that any Pareto-optimal solution can be obtained from this model. We can observe that the trade-off curves varies continuously with λ_1. Therefore, as any solution is Pareto-optimal, we can generate any solution on the Pareto-optimal frontier by choosing the adequate λ_1, and the entire Pareto-optimal set can be obtained by varying λ_1 between 0 and 1.

Along with its benefits, this methods also presents downsides. While the L^4-norm sidelobe level can be kept very low when increasing the SNR, it is less true for the L^∞-norm. We can see on the figure 5.2, representing a particular solution obtained for $\lambda_1 = 0.4$,

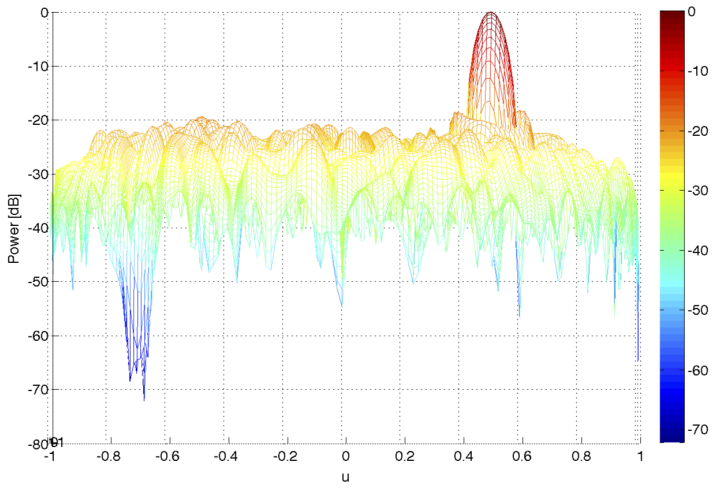

Figure 5.2: Example of solution for $\lambda_1 = 0.4$

	Initial	Perturbed (avg.)
-40dB	-26.8922	-26.8306
-60dB	-26.5556	-26.4604
-80dB	-26.39108	-26.2855

(a) Sidelobe level comparison

	Initial	Perturbed (avg.)
-40dB	0.8877	0.8845
-60dB	0.8740	0.8705
-80dB	0.8668	0.8622

(b) SNR comparison

Figure 5.3: Comparison between the initial and perturbed solutions for different cancellation levels

that the multi-objective algorithm allows higher signal peaks in localised regions. This is especially the case for the first sidelobe, which is significantly higher than the rest of the signal. In the next section, a solution will be proposed to solve this issue by increasing the importance of the region near the main lobe in the minimization function.

We will conclude this section by analyzing the robustness of the multi-objective model, as we suspected in the previous chapter that its particular formulation could make the solution more robust to the weights perturbation. The same process as above was therefore applied in order to quantify this robustness, and the corresponding results can be consulted on tables 5.3 and 5.4. However, the conclusions stay essentially unchanged, whether for the SLL, the SNR or the signal level in the interference region, and we can therefore not conclude to any improvement in that domain.

Target	Maximal	Mean
-40dB	-36.5195	-40.2331
-60dB	-41.3219	-46.3983
-80dB	-42.0320	-48.4589

Figure 5.4: Maximal and mean signal levels in the interference region

5.2 Weighting functions

Until now, when minimizing the sidelobe level, all the regions were given the same importance. However, as seen above, one of the main disadvantages of the L^p-norm minimization over the L^∞-norm minimization is the overtaking of the maximal values in certain regions. This behavior is particularly visible in the region of the first side lobes, and this is even more true with the multi-objective model developed in the last section. It can therefore sometimes be useful to increase the emphasis on certain parts of the domain.

5.2.1 Incorporating weighting functions in the model

A common way to achieve this is to add a weighting function $W(\hat{u})$ on the array pattern in the sidelobe computation. This approach has also been studied in the work of Thibault Clavier et al. mentioned above [13]. In practical, this weighting function $W(\hat{u})$ can be incorporated into the objective the following way :

$$\text{minimize} \iint_{\Omega \setminus \Omega_0} W(\hat{u}) |AP(\hat{u})|^p d\hat{u} \tag{5.3}$$

Concerning our model, the only necessary modification is therefore to compute the coefficients $W(\theta, \phi)$, to include them in the summation terms of the sidelobe level computation, and then proceed similarly as above to build the rest of the model :

$$\text{minimize} \sum_{\Omega \setminus \Omega_0} W(\theta, \phi) |AP(\theta, \phi)|^p \sin\theta \tag{5.4}$$

With this formulation, the convexity property is conserved and the performances of the algorithm are not deteriorated at all. A lot of different weighting functions could be proposed depending on the characteristics required for the solution. In our case, in order to accentuate the importance of the first sidelobes in the SLL computation without neglecting the further regions too much, we will choose weighting functions satisfying the following properties :

- The function should be equal to zero in the interior of the main lobe region

- The function should be maximal at the boundary of the main region, and decrease with the distance to the main region
- The function should be strictly positive everywhere outside of the main region, even for large distances

For this thesis, we will consider two different functions fulfilling these conditions. These functions will be introduced below, we will then compare the results obtained in both cases.

During the rest of the section, for the sake of clarity, the weighting functions will take as argument the ground distance x with respect to the main direction $\hat{u}_0$, instead of the direction $\hat{u}$ itself. This distance can be computed as :

$$x = \sqrt{(u - u_0)^2 + (v - v_0)^2} \tag{5.5}$$

Gaussian function

The first considered weighting function is given by the following expression :

$$W(x) = \begin{cases} e^{-\frac{(x-R_i)^2}{2\sigma^2}} & \text{for } x \geq R_i \\ 0 & \text{for } x < R_i \end{cases} \tag{5.6}$$

with R_i the radius of the main lobe, and σ a parameter chosen by the user. A graphical representation of this function can be found on the graph 5.5, for a particular σ value. We can observe that the relative importance of a particular region in the SLL computation decreases strictly with the distance between this region and the main lobe, getting close to 0 for very far regions. Playing with σ will enable modifying the steepness of the function.

Sinusoidal function

The second function is defined as :

$$W(x) = \begin{cases} \delta + \frac{1-\delta}{2}\left[1 - \sin(\pi(\frac{x - \frac{R_i+R_o}{2}}{R_o - R_i}))\right] & \text{for } R_i \leq x \leq R_o \\ 0 & \text{for } x < R_i \\ \delta & \text{for } x \geq R_o \end{cases} \tag{5.7}$$

with R_o an outer radius larger than R_i, and where δ is a parameter defined arbitrarily by the user. This function is plotted for various x values on graph 5.6. Unlike the previous

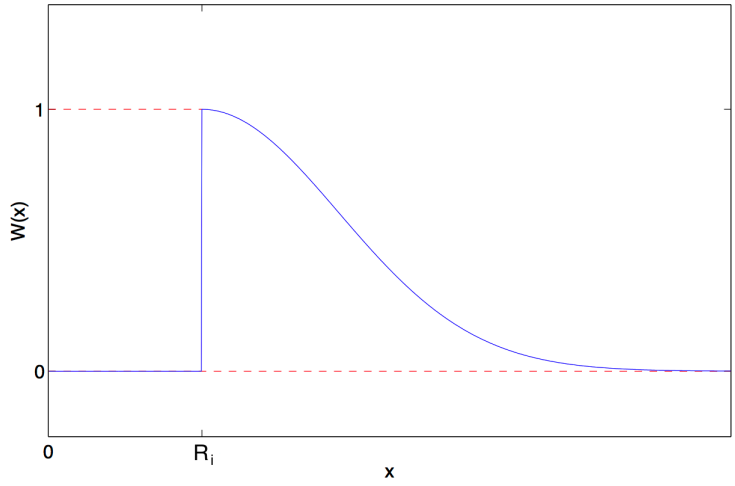

Figure 5.5: Gaussian weighting function

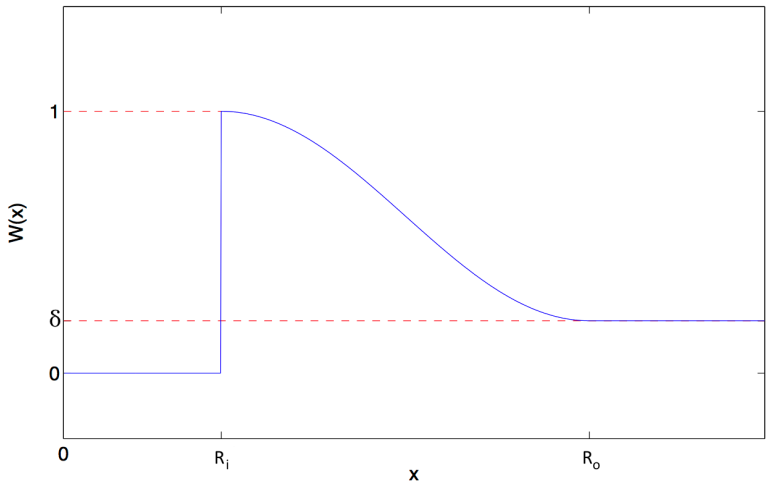

Figure 5.6: Sinusoidal weighting function

one, this function never drops below δ, whatever the distance with the main direction. This way, even the most distant regions are guaranteed to have a relatively significant weight in the sidelobe level computation, avoiding too much signal increase in these areas.

5.2.2 Results analysis

In this section, we will perform an analysis of the solution behavior when a weighting function is applied. For both of the weighting functions presented above, the SLL, SNR and first sidelobe level will be evaluated while varying the functions parameters.

As explained above, the desired effect of the weighting function is to decrease the

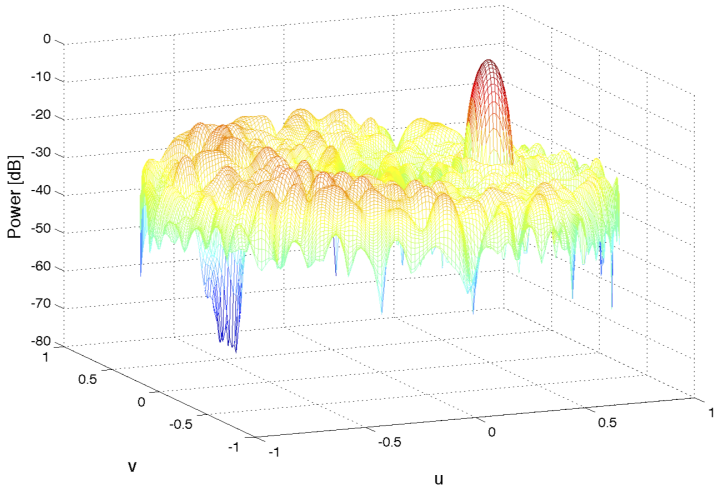

Figure 5.7: Example of solution obtained using a weighting function

signal amplitude in the region close to the main lobe. Of course, it can only be achieved at the price of a slightly higher global SLL. A first example of a solution obtained using a weighting function is displayed on graph 5.7. The relative importance of the region close to the main lobe was voluntarily exaggerated in order to visualize its effects.

In the case of the first function, the first graph of figure 5.8 shows that, for adequate σ values ($\sigma = 0.5$ for instance), an important level decrease can be obtained near the main region, for a relatively small SLL increase elsewhere (in this graph, the red dotted lines represent the value that would be obtained in absence of weighting).

In order to choose the optimal compromise between the SLL and the first lobe level, a possible solution could be to intersect the two corresponding curves on the graph to obtain the same level in both cases (in the L^4-norm sense). However, by looking at the second graph of figure 5.8, we can also observe that the SNR depends directly on σ, and choosing a too low σ value will result in an important drop of this SNR (until 10% of its optimal value in the worst case).

The figure 5.9 displays the results obtained for the second weighting function. This time, the solution behavior will be determined by the parameter δ, representing the minimal weight applied to the far regions. We can directly observe that imposing this lower bound δ enables to decrease the first sidelobe far more efficiently in terms of SLL than in the case of the first function. This is due to the fact that no region is neglected in the objective, which would result in signal peaks in this region and would negatively impact the SLL. In this example, a gain of more than 5 dB could for instance be achieved for the first sidelobe, for an increase of less than half a dB of the SLL.

However, this improvement in terms of SLL goes along with a deterioration of the

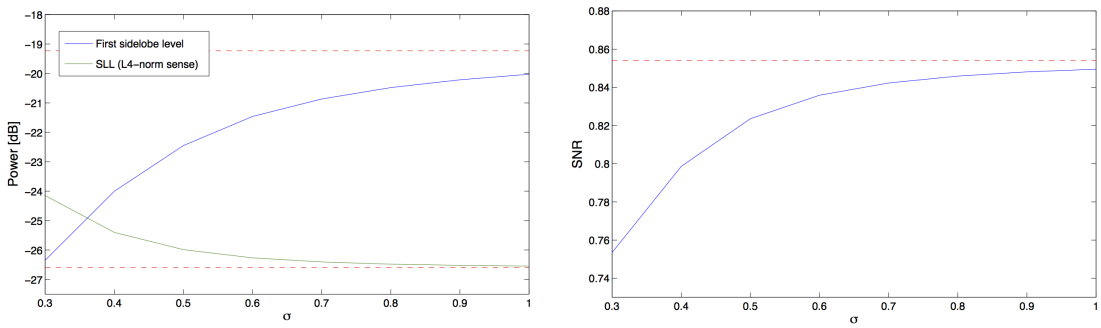

Figure 5.8: Effects of the Gaussian weighting function on the solution

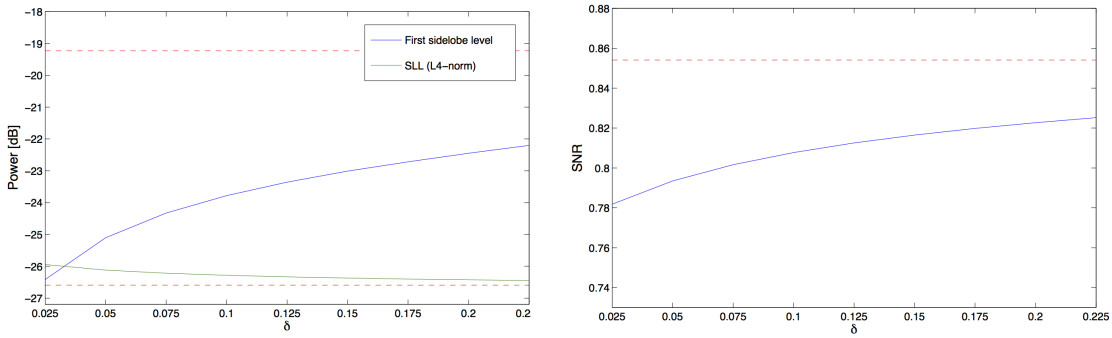

Figure 5.9: Effects of the sinusoidal weighting function on the solution

SNR, as the second graph shows a slight decrease of this SNR compared to the first function.

Finally, let us now inspect the benefits brought by the weighting function on the model built in section 5.1. Of course, as the SLL minimization now only represents a part of the objective, the weighting effect will be diminished relatively to the importance accorded to the SNR maximization.

Three particular situations will be compared. The first one will be the optimal solution for a particular instance, computed with the initial model. The second solution will correspond to the same instance, this time using the multi-objective model with $\lambda_1 = 0.6$. Finally, the last solution will also be obtained from the multi-objective model, but the sinusoidal weighting function will furthermore be applied, with $\delta = 0.125$. The respective SLL, SNR and first sidelobe levels computed for each solution can be consulted on table 5.10.

For this particular instance, we remark that adding the weighting function on the multi-objective model enables to decrease the first sidelobe by almost 2 dB, while increasing the SLL by less than 0.4 dB. Interestingly enough, the SNR appears to be higher for the solution in presence of weighting in this case (although only by a small difference). If we now compare the third solution with the initial model, we achieve a overall gain of about

	SLL	SNR	1^{st} sidelobe level
Initial model	-26.6604	0.8546	-19.2293
Multi-objective model	-26.5859	0.8815	-18.4887
Multi-objective + weighting	-26.2139	0.8833	-20.2401

Figure 5.10: Comparison of the solutions obtained for the different models

3% for the SNR and 1 dB for the first sidelobe, with a decrease of less than half a dB for the sidelobe level. Of course, it is possible to apply completely different parameters than the ones used in this simulation, depending on the user preferences concerning the solution characteristics.

5.3 Power cones

This last section describes another tool to improve the method, this time not in terms of performance (the algorithm will still converge to the same optimal solution) but rather on the formulation efficiency.

We have seen that modelling power L^p-norm constraints could be achieved using second order cones. However, this method can be fastidious for less convenient values of p (typically values that are not powers of 2), and the number of necessary cones can become very important.

However, another types of cones exist (exponential, positive semi-definite, ...). Among them, the power cones offer a very efficient way to reformulate our problem using fewer constraints and variables, which enables reducing significantly the execution time of the algorithm. Furthermore, this formulation also presents the advantage of being same for any value of $p \geq 1$, while the second order cones formulation requires the construction of a new model for each particular value of p.

The power cones are the particular cones satisfying, for a particular $\alpha \in [0, 1]$:

$$\mathcal{P}_n^{\alpha,1-\alpha} = \left\{ x \in \mathbb{R}^n \mid x_1^\alpha x_2^{1-\alpha} \geq \sqrt{\sum_{i \geq 3} x_i^2},\ x_1, x_2 \geq 0 \right\} \tag{5.8}$$

We can observe that the rotated second order cones are a particular case of that definition, for $\alpha = 0.5$.

The complete model can be constructed following the same principles as the second order cones program, only replacing the successive conic constraints by a single power cone constraint. The same reasoning can also be applied for the multi-objective model built above, by combining the use of power cones for the sidelobe minimization, and second

	Second Order Cones	Power Cones
Number of variables	100 425	50 469
Number of linear constraints	49 959	33 307
Number of cones	24 978	8 326

Figure 5.11: Comparison between the SOCP and Power Cones formulations

order cones for the noise power minimization (in that case, the second order cones stay the best choice of cone).

The power cones feature is not yet available in the current version of the MOSEK solver. However, the next version, to be released later this year, has been announced to support the power cones, and the MOSEK support team has kindly agreed to send the alpha version of their software in order to test the model. Unfortunately, this version was not stable enough to generate the expected solutions, due to the complexity of the model and the important number of variables and constraints involved, but we can still perform a complexity comparison of the two formulations, to estimate the gain that could be achieved with the latter.

The differences between the formulations can be consulted on table 5.11. In terms of number of variables, the power cones formulation enables decreasing the total number by 50%. It also reduces the number of linear constraints by more than 30%. Finally, in terms of number of cones, which is crucial due to the complexity of these constraints, we can observe that the power cones formulation requires three times fewer cones than the second order cones formulation.

Considering all these aspects, the new formulation should enable reducing significantly the execution time. Of course, these considerations will also depend on the solver efficiency to deal with power cones.

Chapter 6

Conclusion

All along this thesis, several optimization models were developed with the main purpose of generating optimal weights minimizing the sidelobe level in the L^p-norm sense. The performance analysis of these algorithms enabled us to draw some interesting conclusions.

We saw that the L^p-norm minimization of the sidelobe level presented some significant advantages, compared to the usual L^∞-norm minimization. Firstly, we saw in chapter 3 that this problem could be formulated in a very convenient way using second order cone programming, enabling the use of efficient solvers to obtain globally optimal solutions in a reasonable time (less than 1 minute for a 2° angular resolution). It has furthermore been showed in the following chapter that this L^p formulation enabled to achieve a better SNR and directivity, in addition to minimizing the signal level more globally, and these effects were accentuated when decreasing the value of p.

The final choice of the p value will of course be left to the user. However, this value should be chosen low enough to avoid numerical issues that can sometimes appear for critical instances, but also high enough to avoid higher signal peaks in localized regions.

We also showed in chapter 4 that the model developed was particularly well suited for cancellation of very large regions of the sky. For smaller interference regions, it can be used to cancel the signal pretty deeply. The algorithm showed difficulties for nulling levels deeper than -100 dB, however this has to be put in perspective by the fact than the imperfect precision of the EEP would anyway not enable to maintain such levels in practice.

The robustness analysis showed that the solution was rather robust to the weights perturbations, with very few deterioration of the solution characteristics when subjected to noise, in exception of the interference areas. In these regions, the signal deepness could not maintained deeper than some particular level (depending on the perturbations magnitude), whatever the initially achieved cancellation level. This corroborates the fact that it would not be relevant to impose unreasonable cancellation levels.

Finally, chapter 5 brought additional interesting features to the initial model. The joint optimization of the SLL and SNR enabled to significantly increase the SNR, for a comparatively small loss in terms of SLL. Furthermore, introducing a weighting function enabled to lower the pattern in specific regions, and particularly reduce the first sidelobe level, which was an important downside of the low p norms minimization. Finally, an alternative formulation involving power cones was also provided, expecting to reduce significantly the running time of the algorithm. However, the current state of the available solvers did not allow this to be tested in practice for this thesis.

In order to further improve these methods, it could be interesting to optimize the patterns over a entire range of frequencies, instead of a single one. It would also be appreciable to improve their numerical stability and robustness. This way, all these methods combined together should provide the astronomers an improved freedom of choice concerning the characteristics of the solutions obtained by the algorithms, and a better adaptation potential to the diversity of the situations that could be encountered in real life.

Bibliography

[1] "The SKA Project." `https://www.skatelescope.org/the-ska-project/`, 2018.

[2] C. Craeye, "Lecture notes of LELEC2910 : Antennas and Propagation." Université Catholique de Louvain.

[3] "By Original JPG (File:Felder um Dipol.jpg) due to Averse, SVG by Maschen. [CC0], from Wikimedia Commons."

[4] Q. Gueuning, C. Raucy, C. Craeye, E. Colin-Beltran, and E. de Lera Acedo, "Mutual coupling analysis in non-regular arrays of skala antennas with the harp approach," in *Antennas and Propagation & USNC/URSI National Radio Science Meeting, 2015 IEEE International Symposium on*, pp. 1528–1529, IEEE, 2015.

[5] H. Bui-Van, J. Abraham, M. Arts, Q. Gueuning, C. Raucy, D. Gonzalez-Ovejero, E. de Lera Acedo, and C. Craeye, "Fast and accurate simulation technique for large irregular arrays," *IEEE Transactions on Antennas and Propagation*, vol. 66, no. 4, pp. 1805–1817, 2018.

[6] B. D. Van Veen and K. M. Buckley, "Beamforming: A versatile approach to spatial filtering," *IEEE assp magazine*, vol. 5, no. 2, pp. 4–24, 1988.

[7] D. H. Johnson and D. E. Dudgeon, *Array signal processing: concepts and techniques*. PTR Prentice Hall Englewood Cliffs, 1993.

[8] H. L. Van Trees, *Optimum array processing: Part IV of detection, estimation, and modulation theory*. John Wiley & Sons, 2004.

[9] H. Lebret and S. Boyd, "Antenna array pattern synthesis via convex optimization," *IEEE transactions on signal processing*, vol. 45, no. 3, pp. 526–532, 1997.

[10] H. Lebret, "Optimal beamforming via interior point methods," *Journal of VLSI signal processing systems for signal, image and video technology*, vol. 14, no. 1, pp. 29–41, 1996.

[11] V. Hamaide, "Optimal interference nulling for large arrays of coupled antennas," Master's thesis, Université Catholique de Louvain, 2018.

[12] P. Gerstoft and W. S. Hodgkiss, "Improving beampatterns of two-dimensional random arrays using convex optimization," *The Journal of the Acoustical Society of America*, vol. 129, no. 4, pp. EL135–EL140, 2011.

[13] T. Clavier, N. Razavi-Ghods, F. Glineur, D. Gonzalez-Ovejero, E. de Lera Acedo, C. Craeye, and P. Alexander, "A global-local synthesis approach for large non-regular arrays," *IEEE Transactions on Antennas and Propagation*, vol. 62, no. 4, pp. 1596–1606, 2014.

[14] E. de Lera Acedo, N. Razavi-Ghods, N. Troop, N. Drought, and A. Faulkner, "Skala, a log-periodic array antenna for the ska-low instrument: design, simulations, tests and system considerations," *Experimental Astronomy*, vol. 39, no. 3, pp. 567–594, 2015.

[15] A. El-Makadema, L. Rashid, and A. K. Brown, "Geometry design optimization of large-scale broadband antenna array systems," *IEEE Transactions on Antennas and Propagation*, vol. 62, no. 4, pp. 1673–1680, 2014.

[16] F. Glineur, "Lecture notes of LINMA2471 : Optimization models and methods II." Université Catholique de Louvain.

[17] S. Boyd and L. Vandenberghe, *Convex optimization*. Cambridge university press, 2004.

[18] Y. Morenko, A. Vinel, Z. Yu, and P. Krokhmal, "On p-norm linear discrimination," *European Journal of Operational Research*, vol. 231, no. 3, pp. 784–789, 2013.

[19] F. Alizadeh and D. Goldfarb, "Second-order cone programming," *Mathematical programming*, vol. 95, no. 1, pp. 3–51, 2003.

[20] A. Ludwig, "The definition of cross polarization," *IEEE Transactions on Antennas and Propagation*, vol. 21, no. 1, pp. 116–119, 1973.

[21] "MOSEK Optimization Toolbox for MATLAB 8.1.0.60." `https://docs.mosek.com/8.1/toolbox/index.html`, 2018.

[22] V. Rabinovich and N. Alexandrov, *Antenna arrays and automotive applications*. Springer Science & Business Media, 2012.

[23] H. Cox, R. Zeskind, and M. Owen, "Robust adaptive beamforming," *IEEE Transactions on Acoustics, Speech, and Signal Processing*, vol. 35, no. 10, pp. 1365–1376, 1987.

[24] A. Ben-Tal, L. El Ghaoui, and A. Nemirovski, *Robust optimization*, vol. 28. Princeton University Press, 2009.

[25] R. T. Marler and J. S. Arora, "Survey of multi-objective optimization methods for engineering," *Structural and multidisciplinary optimization*, vol. 26, no. 6, pp. 369–395, 2004.

[26] K. Miettinen, *Nonlinear multiobjective optimization*, vol. 12. Springer Science & Business Media, 2012.

[27] S. Jayaprakasam, S. K. A. Rahim, C. Y. Leow, T. O. Ting, and A. A. Eteng, "Multiobjective beampattern optimization in collaborative beamforming via nsga-ii with selective distance," *IEEE Transactions on Antennas and Propagation*, vol. 65, no. 5, pp. 2348–2357, 2017.

Appendix A

Second Order Cone model for $p = 6$

$$
\begin{aligned}
&\text{minimize} && t && \\
&\text{subject to} && \sum_{i \in \Omega \backslash \Omega_0} s_i \sin(\theta) \leq t && \\
& && x_i^2 \leq w_i && \text{on } \Omega \\
& && w_i^2 \leq s_i x_i && \text{on } \Omega \\
& && {Z_{H,i}^r}^2 + {Z_{H,i}^{im}}^2 + {Z_{V,i}^r}^2 + {Z_{V,i}^{im}}^2 \leq x_i && \text{on } \Omega \\
& && Z_H^r = \mathbf{P}_H^r \mathbf{w}^r - \mathbf{P}_H^{im} \mathbf{w}^{im} && \text{on } \Omega \\
& && Z_H^{im} = \mathbf{P}_H^r \mathbf{w}^{im} + \mathbf{P}_H^{im} \mathbf{w}^r && \text{on } \Omega \\
& && Z_V^r = \mathbf{P}_V^r \mathbf{w}^r - \mathbf{P}_V^{im} \mathbf{w}^{im} && \text{on } \Omega \\
& && Z_V^{im} = \mathbf{P}_V^r \mathbf{w}^{im} + \mathbf{P}_V^{im} \mathbf{w}^r && \text{on } \Omega \\
& && \mathbf{P}_{co}^r \cdot \mathbf{w}^r - \mathbf{P}_{co}^{im} \cdot \mathbf{w}^{im} = 1 && \text{for } (\theta_0, \phi_0) \\
& && \mathbf{P}_{co}^r \cdot \mathbf{w}^{im} + \mathbf{P}_{co}^{im} \cdot \mathbf{w}^r = 0 && \text{for } (\theta_0, \phi_0) \\
& && x_i \leq C^2 && \text{on } \Omega_i \\
& && x_i \leq 1 && \text{on } \Omega_0 \\
& && x_i \leq 0.5 && \text{on } \Omega_{hp} \backslash \Omega_0
\end{aligned}
$$

Rue Archimède, 1 bte L6.11.01, 1348 Louvain-la-Neuve, Belgium **www.uclouvain.be/epl**